

Research Articles | Systems/Circuits

CCKergic Tufted Cells Regulate Odor Sensitivity by Controlling Mitral Cell Output in the Mouse Olfactory Bulb

<https://doi.org/10.1523/JNEUROSCI.1243-24.2025>

Received: 22 June 2024

Revised: 11 February 2025

Accepted: 3 March 2025

Copyright © 2025 Starr et al.

This is an open-access article distributed under the terms of the [Creative Commons Attribution 4.0 International license](#), which permits unrestricted use, distribution and reproduction in any medium provided that the original work is properly attributed.

This Early Release article has been peer reviewed and accepted, but has not been through the composition and copyediting processes. The final version may differ slightly in style or formatting and will contain links to any extended data.

Alerts: Sign up at www.jneurosci.org/alerts to receive customized email alerts when the fully formatted version of this article is published.

1 **Title:** CCKergic Tufted Cells Regulate Odor Sensitivity by Controlling Mitral
2 Cell Output in the Mouse Olfactory Bulb

3 **Abbreviated title:** CCKergic tufted cells control OB output and odor
4 detection

5 **Author:** Eric Starr[†], Rashika Budhathoki[†], Dylan Gilhooly[†], Laura Castillo[†],
6 Meigeng Hu[‡], Dan Zhao[‡], Yaping Li[‡], Shaolin Liu^{†,‡}

7
8 [†]Department of Anatomy, Howard University, Washington, DC 20059

9 [‡]Center for Neurological Disease Research, Department of Physiology and
10 Pharmacology, Department of Biomedical Sciences, University of Georgia
11 College of Veterinary Medicine, Athens, GA 30602

12
13 **Corresponding author email:** shaolin.liu@uga.edu

14 **Number of pages:** 56

15 **Number of figures:** 12

16 **Number of words:** 249 (abstract)

17 641 (introduction)

18 1585 (discussion)

19 **Conflict of interest statement:** The authors declare no competing
20 financial interests.

21

22 **Acknowledgments:** We thank Ms. Corinne A. Perloski for her assistance
23 in animal care and maintenance. This work was supported by NIH Grants
24 R01DC14447, RF1AG069196, R01AG074216, R01AG077541.

25

26 **ABSTRACT**

27 Despite the importance of odor detection to the survival of most animals,
28 mechanisms governing olfactory sensitivity remain unclear, especially beyond the
29 olfactory sensory neurons (OSNs). Here we leverage opto- and chemo-genetics to
30 selectively modulate activities of CCKergic tufted cells (TCs) in the mouse olfactory bulb
31 (OB) of either sex, which form the intrabulbar associational system (IAS) to link
32 isofunctional glomeruli, to determine the functional impact on OB output via mitral cells
33 (MCs) and odor detection in behaving animals. NMDA receptors in CCKergic TCs
34 remarkably amplify the OSN-evoked monosynaptic responses in these excitatory
35 neurons, which provide a long-lasting feedforward excitation to MCs via both chemical
36 transmission and electrical synapses between their apical dendrites. NMDA receptors in
37 MCs mediate late components of the dendrodendritic TC→MC transmission to
38 significantly boost MC outcome. Congruently, optogenetic inhibition of the CCKergic
39 TCs dramatically reduces the OSN-evoked MC responses. Unexpectedly, optogenetic
40 activation of the axons projecting from CCKergic TCs on the opposite side of the same
41 bulb produces a mainly AMPA receptor-mediated excitatory responses in MCs, leading
42 us to speculate that CCKergic TCs functionally synchronize MC output from mirror
43 glomeruli. Furthermore, chemogenetic inhibition of CCKergic TCs reduces animal's
44 sensitivity to odors by elevating detection threshold, consistent with the key role of these
45 TCs in functionally controlling MC output. Collectively, our results delineate the cellular
46 and circuit mechanisms allowing the CCKergic TCs to regulate MC output from
47 glomeruli on both medial and lateral side of each OB and the system's sensitivity to
48 odors possibly via the IAS.

49 **Significance Statement**

50 The detection and processing of chemical stimuli, such as environmental odorants, are
51 essential for the central nervous system to generate appropriate behavioral responses
52 in animals. Most of our current knowledge about odor detection comes from studies on
53 the interactions between chemical stimuli and odorant receptors on olfactory sensory
54 neurons (OSNs) at the periphery. In this study, we have identified a specific
55 subpopulation of nerve cells that play a crucial role in converting sensory input into
56 biological signals within the olfactory bulb, the downstream target of OSNs and the
57 initial site of synaptic odor processing. Our findings provide new insights into the cellular
58 and circuit-level mechanisms that regulate olfactory detection beyond sensory neurons.

59

60

61

62

63

64

65

66

67

68 INTRODUCTION

69 Given the importance of detecting chemical stimuli in the environment to the
70 survival of most animals (Lledo et al., 2005), understanding how the olfactory system
71 governs its sensitivity to odorants is of paramount significance. Previous studies on this
72 topic mainly focused on odorant receptors (ORs) on olfactory sensory neurons (OSNs)
73 in the olfactory epithelium (van Drongelen et al., 1978; Meisami, 1989; Apfelbach, 1991;
74 Dekker et al., 2006; Dewan et al., 2018). However, the neurobiological mechanisms
75 underlying olfactory sensitivity and odor detection beyond OSNs are less explored.

76 Anatomically, OSNs project axons to the olfactory bulb (OB), where their axons
77 terminate and form synapses with projection neurons and local interneurons (Buck,
78 1996; Lledo et al., 2005; Nagayama et al., 2014; Mori and Sakano, 2021). Each OSN
79 expresses a single type of ORs out of a repertoire of ~1100 members in rodents and
80 ~400 in humans (Buck and Axel, 1991). OSNs expressing the same type of ORs project
81 their axons precisely and reproducibly to a pair or few of glomeruli located on the medial
82 and lateral side of each OB (Ressler et al., 1994; Vassar et al., 1994; Mombaerts et al.,
83 1996). These glomeruli are simultaneously activated by the same odorants thus termed
84 mirror or isofunctional glomeruli (Rubin and Katz, 1999; Lodovichi et al., 2003; Zou et
85 al., 2009). Since its discovery decades ago, the physiological significance of this unique
86 structural arrangement has remained unclear.

87 Prior to the experimental demonstration of mirror glomeruli, a neural circuit
88 termed intrabulbar associational system (IAS) reciprocally connecting the medial and
89 lateral sides of each OB was anatomically characterized in hamsters (Schoenfeld et al.,

90 1985). IAS is predominantly formed by subpopulation of tufted cells with somata located
91 in the superficial portion of the external plexiform layer (EPL) thus called superficial
92 tufted cells (STCs). These STCs are topographically organized to have single apical
93 dendrites ramifying in individual glomeruli and axons projecting to the internal plexiform
94 layer (IPL) where they course abruptly and travel along to the opposite side of the same
95 OB terminating in the IPL right beneath the mirror glomeruli. This STC-formed unique
96 neural circuitry was subsequently demonstrated in rats and mice to link mirror glomeruli
97 (Liu and Shipley, 1994; Belluscio et al., 2002; Lodovichi et al., 2003). Furthermore, the
98 IAS refinement exhibits high level of activity-dependent plasticity (Marks et al., 2006;
99 Cummings and Belluscio, 2010), indicating active IAS participation in olfactory
100 processing. Thus, elucidating the functional mechanisms underlying the IAS operation
101 will potentially shed light on the biological significance of mirror glomeruli organization in
102 the olfactory system.

103 To explore the principles governing the functional operation of IAS, it is important
104 to understand the synaptic interactions between the IAS-forming STCs and the circuit-
105 related neurons. Since the IAS-forming STCs exclusively express the neuropeptide
106 cholecystokinin (CCK) (Liu and Shipley, 1994), this enables us to utilize it as a
107 molecular marker to selectively label and manipulate activities of these cells and the IAS
108 circuit with optogenetic and chemogenetic approaches and analyze the functional
109 readout of other local neurons and animals' behavioral outcome. For example, recent
110 studies with these approaches have revealed that IAS-forming STCs actively recruit
111 local GABAergic interneurons (Sun et al., 2020) and participate in odor detection (Chen
112 et al., 2024). However, the cellular and circuit mechanisms underlying the roles of these

113 CCKergic tufted cells in odor detection remain to be elusive. Given the ramification in
114 individual glomeruli by apical dendrites of both CCKergic STCs and mitral cells (MCs),
115 we hypothesize that CCKergic STCs interact with MCs and modulate their output. To
116 test this, we designed and completed a series of experiments with clear demonstration
117 of CCKergic TC's role in intermediating feedforward monosynaptic excitation to MCs on
118 both sides of each OB to regulate OB output to downstream centers thus enabling the
119 system to detect weak signals by increasing odor detection sensitivity at the cellular and
120 circuit levels in the OB.

121 **METHODS**

122 **Animals**

123 Wild-type (C57BL/6J) and transgenic, homozygous CCK-Cre mice were obtained
124 from The Jackson Laboratory (Bar Harbor, ME). Homozygous CCK-Cre mice (CCK-
125 Cre+/+) were maintained by breeding male and female CCK-Cre+/+ mice.
126 Heterozygous CCK-Cre (CCK-Cre+/-) mice were generated by breeding male
127 homozygous CCK-Cre mice and female wild-type C57BL/6J mice. Animals were
128 maintained with a standard 12 h light/dark cycle with water and food ad libitum. All
129 experimental procedures were performed in accordance with approval from the
130 Institutional Animal Care and Use Committee of Howard University and the University
131 of Georgia.

132 **Surgical Procedures and Viral Injection**

133 Stereotaxic viral injections were performed as previously described (Sun et al.,
134 2020). Briefly, animals were deeply anesthetized by an initial intraperitoneal (i.p.) dose

135 of 100 mg/kg ketamine and 10 mg/kg xylazine mixture before the skull was exposed
136 and a craniotomy (1mm) was drilled on the midline between two bulbs at 3.95 mm from
137 Bregma. For all experiments, injections were localized to the superficial EPL of the OB.
138 The coordinates for injection in the medial OB was 0.3 mm from the midline, 1.5 mm
139 depth from the OB dorsal surface. For the lateral OB injection, the coordinates were 1.2-
140 1.3 mm from midline at a depth 1.2-1.3 mm from OB dorsal surface. For
141 electrophysiological experiments, mice (4-6 weeks of age) were injected in the
142 superficial EPL on the medial side of the OB with one of the following: Adeno-
143 associated virus (AAV) serotype 5 carrying fusion genes for the fluorescent protein
144 tdTomato, channelrhodopsin 2 and enhanced yellow fluorescent protein (AAV5-ChR2-
145 EYFP), or halorhodopsin (eNpHR 3.0) and EYFP (AAV-HR-EYFP). For behavioral
146 experiments, we utilized the Designer Receptors Exclusively Activated by Designer
147 Drugs (DREADDs). Mice (4-5 weeks) were injected with AAV5 carrying fusion gene
148 encoding the inhibitory DREADD hM4D(Gi) and the fluorescent protein mCherry into the
149 medial portion of the OB (AAV-hM4Di-mCherry). AAV injections were conducted by a
150 nanoliter injector (Nanoject III, Drummond Scientific, Broomall, PA) at rate of 10 nL/sec.
151 All animals recovered for 4-6 weeks to ensure viral expression prior to the onset of
152 experiments. All viruses were purchased from Addgene (Watertown, MA.)

153 **Slice Preparation**

154 For electrophysiological experiments, OB slices were obtained from 8–10-week-
155 old male and female mice. Animals were anesthetized with isoflurane prior to
156 decapitation and OBs were rapidly dissected and mounted onto a VT1200S Vibratome
157 disc (Leica, Nussloch Germany) using superglue. Horizontal or coronal OB slices (350

158 μM) were cut in oxygenated (95% O_2 -5% CO_2) ice cold sucrose-ACSF containing (in
159 mM): 210 sucrose, 2.0 KCl, 1.25 NaH_2PO_4 , 26 NaHCO_3 , 10 Glucose, 8 MgSO_4 , 0.5
160 CaCl_2 . Slices were immediately transferred to and incubated in continuously
161 oxygenated ACSF which were heated to 30°C and had the following composition (in
162 mM): 124 NaCl, 2.5 KCl, 1.25 NaH_2PO_4 , 6.0 MgSO_4 , 2.0 CaCl_2 , 26 NaHCO_3 , 10
163 glucose. Following incubation, slices were transferred to and maintained for at least 30
164 min at room temperature in normal ACSF containing (in mM): 124 NaCl, 2.5 KCl, 1.25
165 NaH_2PO_4 , 2.0 MgSO_4 , 2.0 CaCl_2 , 26 NaHCO_3 , 10 glucose, before being used for
166 recordings. In the recording chamber, slices were perfused at 3ml/min with continuously
167 oxygenated ACSF warmed to 30°C .

168 **Electrophysiology**

169 Whole-cell patch clamp recordings were made from OB neurons visualized via an
170 Axio Examiner.A1 (Zeiss, Jena, Germany) upright epifluorescence microscope
171 equipped with near-infrared differential interference contrast (IR-DIC) optics.
172 Visualization of neurons was obtained by loading patch pipettes with 5 μM Alexa fluorTM
173 594 (AF 594). Mitral cells (MCs) were identified by their somatic localization to the mitral
174 cell layer and the presence of their apical and lateral dendrites projecting into the EPL
175 (Macrides and Schneider, 1982; Burton and Urban, 2014; Liu et al., 2016). STCs were
176 identified by their somatic localization within the superficial EPL and the presence of
177 one or more lateral dendrites (Liu and Shipley, 1994; Sun et al., 2020). For post-hoc
178 reconstruction of the recorded neurons, 0.2% neurobiotin was included in the patch
179 pipette solution.

180 Current and voltage signals were recorded with a MultiClamp 700B amplifier
181 (Molecular Devices, Palo Alto, CA), and low-pass filtered at 4 kHz and sampled at 10
182 kHz with a DIGIDATA 1550B 16-bit analog-to-digital converter using Clampex 11.1
183 software (Molecular Devices). Patch recording electrodes (4-10 M Ω) were pulled from
184 thin-wall glass capillary tubes with filament (Sutter Instrument, Novato, CA). For current-
185 clamp whole-cell recording, patch pipettes contained (in mM): 122 K-gluconate, 4
186 EGTA, 0.5 CaCl₂, 5 MgCl₂, 10 HEPES, 3 Na₂-ATP, 0.3 Na₃-GTP, 10 Tris-
187 phosphocreatine (285-295 mOsm, pH 7.27 with KOH). In some cases, depolarizing
188 current was injected to maintain a recorded MC at a membrane potential near the action
189 potential threshold. To record spontaneous and evoked excitatory postsynaptic currents
190 (EPSCs), patch pipettes were filled with a recording solution containing (in mM): 133
191 CsCH₃O₃S, 3 EGTA, 0.4 CaCl₂, 5 QX-314, 4 MgCl₂, 10 HEPES, 3 Na₂-ATP and 0.3 Na₃-GTP
192 (285-295 mosm, pH 7.27 with CsOH). All cells were held between -50 mV to permit
193 study of both NMDAR- and AMPAR-mediated synaptic events.

194 **Electrical and Optical Stimulation**

195 Electrical stimulation of the olfactory nerve (ON) was delivered by a bipolar
196 stimulation electrode, which were made from theta borosilicate tubes and filled with
197 ACSF. Isolated and constant current pulses (0.1 ms) were triggered by a Master-9 pulse
198 stimulator with an ISO-FLEX stimulus isolator (AMPI, Jerusalem, Israel). Optical
199 stimulation was produced by a Polygon 400E illuminator (Mightex, Toronto, Canada),
200 which enables localized stimulation to distinct regions of the OB. Both the size of the
201 optic window and intensity of the optic stimulation were coordinated via Polyscan
202 software (Mightex, Toronto, Canada). The size of the optic window varied depending on

203 experiments, ranging from 20-30 μM rectangle for internal plexiform stimulation (IPL)
204 stimulation to 90 μM diameter for glomerular stimulation. Validation of lack of ChR2
205 expression on MCs was performed by setting a circular optic window over the cell body
206 alone (20-30 μM in diameter) and cells exhibiting responses following optic stimulation
207 (1 ms) were interpreted as internal tufted cells thus were discarded from the final
208 results. For optical stimulation of STC apical dendrites, a circular optic window
209 (diameter of 90 μM) was placed at glomeruli localized containing the apical dendrites of
210 a recorded MC. Finally, for IPL stimulation a circular optic window was placed directly
211 under the recorded MC (diameter 30 μM) and stretched from the superficial IPL to the
212 deep IPL. Onset and duration of optical stimulation were measured by the same
213 MultiClamp 700B amplifier and monitored throughout the duration of the experiment.

214 **Drug application**

215 All drugs, unless noted otherwise, were bath applied during experiments. D-2-
216 Amino-5-phosphonopentanoic acid sodium salt (APV, 50 μM), and 6,7-Dinitroquinoxaline-2,3-
217 dione disodium salt (DNQX, 20 μM) were purchased from Tocris Cookson (Ellisville, MO).
218 Clozapine-N-oxide (CNO) dihydrochloride was purchased from HelloBio (Bristol, UK) and
219 dissolved in DI water as stock solution before being diluted to final concentration with ACSF or
220 sterile saline for bath application (10 μM) in electrophysiological experiments or i.p. injections (3
221 mg/kg body weight) for in vivo behavioral studies, respectively. Given its elimination half-life of
222 ~ 7.5 hours (Guitton et al., 1998; Allen et al., 2019; Jendryka et al., 2019), animals received a
223 dose of CNO ip injection every 8 hours in the two-bottle discrimination test as described below.
224 In other behavioral tests, a single CNO injection was delivered 30 min before the test
225 started (Jendryka et al., 2019). Neurobiotin was purchased from Vector Laboratories
226 (Burlingame, CA). CY3-conjugated to Streptavidin was purchased from Jackson

227 ImmunoResearch Laboratories Inc. (West Grove, PA). Alexa Fluor™ 594 hydrazide was
228 purchased from ThermoFisher (Waltham, MA). All other drugs were purchased from Sigma-
229 Aldrich (St. Louis, MO). All drugs were dissolved in deionized (DI) water as stock solutions and
230 diluted in ACSF to their final concentrations.

231

232 *Behavioral Studies*

233 *Buried Food Test* This test is to assess the animal's detection of food odors (Yang and
234 Crawley, 2009; Machado et al., 2018). In two consecutive days prior to the test, animals
235 were individually housed with a piece of cookie (~1 gram) placed in their cages for them
236 to consume. Then mice were food-deprived for 24 hours before the test, during which a
237 mouse was placed in a clean test cage containing 1 inch of clean bedding material to
238 acclimate for 10 min. After the mouse was removed from the test cage, and a piece of
239 cookie was buried at a random location under the bottom of the bedding material. The
240 test started by reintroducing the mouse to the test cage and recording the time taken for
241 the animal to retrieve the cookie. For those failing to identify the buried cookie in 10 min,
242 600 s was assigned as their latency score. All animals foraged for food by active
243 searching and digging in the test cage, suggesting that fasting sufficiently motivate
244 animals to perform the test. As the control experiment testing animal's visual ability to
245 identify the food source, the latency for each animal to identify the visible cookie placed
246 on the top of bedding material in the same test cage was also recorded at the end of
247 each BFT experiment.

248 *Two-bottle Discrimination Test*

249 As previously described (Wysocki et al., 1977; Pourtier and Sicard, 1990; Griff and
250 Reed, 1995), this assay measures the animal's ability to detect the presence of a
251 monomolecular odorant at progressively decreased concentrations in the drinking
252 solution thus is considered as an odor detection threshold test. Briefly, mice were singly
253 housed with no water supply but restricted access to a bottle of saccharin-phthalic acid
254 solution (SPS, 2.1×10^{-2} M sodium saccharin and 10^{-3} M phthalic acid) for 1 hour twice
255 a day for 2 consecutive days to ensure that they would start drinking when the solution
256 bottle was available. On the 3rd day, animals were given a bottle containing SPS with
257 10^{-3} M isovaleric acid (iVA), which has a robustly distinctive odor, for 10 min.
258 Immediately after exposure to and drinking iVA-containing SPS, each mouse received a
259 single dose (15 μ l/g body weight) of intraperitoneal (i.p.) injection of 0.6 M LiCl to induce
260 an aversive state, and was returned to a clean cage. Two hours later, each mouse was
261 provided two bottles, one with SPS and the other with the same solution containing 10^{-3}
262 M iVA. For every 24 hours, the fluid consumption amount from each bottle by individual
263 animal was determined by weighing bottles followed by iVA concentration reduction by
264 10-fold/24 hr from 10^{-3} M to 10^{-7} M as the experiment continued for 5 consecutive days.
265 The positions of the odorized versus non-odorized bottles in each cage reversed every
266 12 hours to minimize confound effects due to animal's location preference or memory.
267 An index of preference to the odorized solution for each iVA concentration was
268 calculated as the amount of the iVA-odorized solution consumed divided by the total
269 amount of liquid consumed for each mouse over the corresponding 24-hour test
270 period.

271 *Open field test*

272 This behavioral paradigm is based on the idea that mice naturally prefer to explore near
273 a protective wall rather than an open area to expose to potential dangers thus is utilized
274 to assess animal's locomotion activities and anxious behavior (Seibenhener and
275 Wooten, 2015). A square transparent test box (60cm x 60cm x 25cm) is made out of
276 plexiglass with a digital center area (30cm x 30cm) drawn in the video tracking program
277 AnyMaze. Each animal was introduced to the box center followed by video recording for
278 ten minutes. Overall activity in the test box, the amount of time and distance traveled in
279 the center area of the test box were measured and analyzed.

280 **Immunohistochemistry**

281 TO examine ChR2-YFP, hM₄D(Gi)-mCherry, or HR-YFP expression in the OB at
282 3-4 weeks after AAV microinjection, mice were anesthetized and transcardially perfused
283 with 4% paraformaldehyde (PFA) before the OB tissue was prepared for
284 immunohistochemistry as described previously (Liu et al., 2013; Liu and Liu, 2018).
285 Whole OBs were dissected out and kept in 4% PFA at 4°C overnight. PFA was replaced
286 in < 24 h after perfusion with phosphate-buffered saline (PBS). For additional
287 preservation of OBs for <7d, PBS was replaced with long-term protectant solution
288 containing X. Coronal OB sections (50 μm thickness) were cut using a Compressome
289 VF-310-0Z (Precisionary Instruments, Greenville, NC) and kept in PBS at room
290 temperature (RT). OB sections were then transferred to 6-well culture dishes and rinsed
291 with PBS 3x's (5 min/each) after gentle shaking. Slices were then incubated in a 0.1 M
292 PB solution containing 4',6-diamidino-2-phenylindole (DAPI) (5 μg/ml) at room
293 temperature in the dark for 10 min with gentle shaking. After washed with PBS (5 min

294 each) for 3 times, sections were wet mounted and cover-slipped with fluorescence
295 mounting media. Coverslip-mounted slides were stored at 4°C in the dark until imaging
296 with confocal microscopy.

297 Horizontal or coronal OB slices (350 μm) containing neurobiotin filled neurons in
298 electrophysiological experiments were kept in 4% PFA at 4°C overnight. Slices were
299 washed for three times (5 min/each) with PBS and incubated for 1 hour at RT with
300 gentle shaking in a blocking solution made by PBS containing 1% (w/v) bovine serum
301 albumin (BSA) and 0.5% (v/v) Triton X-100. After being transferred to and incubated in
302 the same blocking solution containing streptavidin-CY3 (1 $\mu\text{g}/\text{ml}$) covered with
303 aluminum foil to prevent light exposure at RT on a shaker for 7 h, slices were washed
304 3x's in PBS (5 min/each) to rinse streptavidin-CY3. DAPI staining followed by section
305 mounting were performed as described above.

306 Fluorescent images of fixed slices were captured using a Nikon Ti-E-PFS (Nikon,
307 Japan) inverted spinning-disk confocal microscope equipped with 20x and 40x 1.4NA
308 Plan Apo Lambda objectives or a Zeiss LSM 900 Confocal Microscope with AI sample
309 finder equipped with 2.5x/0.085 and 40x/1.4 objectives. The Nikon system is outfitted
310 with a Yokogawa CSU-X1 (Yokogawa Electric, Japan) spinning disk unit, a self-
311 contained 4-line laser module (excitation at 405, 488, 561, and 640nm), and
312 Andor iXon 897 EMCCD camera. The Zeiss system has four diode lasers (405nm, 488
313 nm, 561 nm and 640 nm) for fluorescence excitation and four fluorescence filters for
314 imaging (blue for DAPI, green for GFP or YFP, red or far red for mCherry or CY5).

315 Fluorescence images of OB sections (50 μ m) were collected and exported as Tiff file
316 format.

317 **Statistical Analysis**

318 All numerical data are presented as the mean \pm SEM. Both action potential and
319 EPSC events were detected in Clampfit 11.1. Action potential detection threshold was
320 set to -30 mV to exclude EPSP detection. Minimal membrane potential was measured
321 as described previously (Liu and Shipley, 2008). EPSC detection threshold was set just
322 below baseline to permit evaluation of area under the curve, and amplitude of EPSCs.
323 Group data were plotted with Origin Pro 2020 (Origin Lab, Northampton, MA). The ON-
324 evoked burst duration in current clamp was measured as the time difference between
325 the peak time of the first action potential and the last one in each response. Statistical
326 significance for electrophysiological experiments ($p < 0.05$) was assessed using
327 Student's t-test, or one-way repeated measure ANOVA with a Bonferroni post hoc
328 comparisons. Paired student's tests were used for comparing data in the presence and
329 absence of distinct drugs (DNQX, APV, and CBX) in the same populations of cells.
330 Behavioral tests were assessed with a One-Way ANOVA with Bonferroni post hoc
331 comparisons.

332 **RESULTS**

333 **Predominant targeting the CCKergic superficial tufted cells**

334 The neuropeptide CCK has been detected in cells of different OB layers (Seroogy et al.,
335 1985) but with a predominant distribution in the superficial EPL in rats (Liu and Shipley,
336 1994). A similar distribution pattern of CCKergic neurons has been reported in the OB of

337 transgenic CCK-Cre mice, which express the Cre recombinase under the CCK promoter
338 thus enables selective labeling, optogenetic or chemogenetic manipulation of these
339 CCK-containing neurons (Sun et al., 2020; Chen et al., 2024). Although a general
340 consensus is that CCK is only expressed by TCs in the OB, previous studies with the
341 same transgenic CCK-Cre mice reported a varied percentage of labeling each out of
342 four subpopulations of TCs (Marks et al., 2006; Cheetham et al., 2015; Economo et al.,
343 2016; Short and Wachowiak, 2019; Sun et al., 2020; Zak and Schoppa, 2021; Chen et
344 al., 2024), which are termed as external (eTCs), superficial (sTCs), middle (mTCs) and
345 deep tufted cells (dTTCs) based on their cell body location in the OB. This variation may
346 reflect the differences in multiple experimental variables including substrains of animals
347 used (homozygotes vs hemizygotes), labeling approaches (animal crossing and viral
348 transfection), animal age for virus injection, and viral serotypes. Our previous work
349 showed a predominant labeling of superficial TCs in the EPL with a viral transfection
350 approach (Sun et al., 2020). However, due to our lack of quantifying eTCs, a
351 subpopulation of TCs providing direct feedforward excitation to MCs (De Saint Jan et
352 al., 2009; Najac et al., 2011; Gire et al., 2012) and exhibiting a remarkable labeling in a
353 recent study with the same animal model (Zak and Schoppa, 2021), we performed this
354 experiment to reassess the relative labeling of four different subpopulations of TCs
355 including eTCs. Since TCs are mainly classified by their soma location, we chose Cre-
356 dependent AAV5-FLEX-tdTomato of the CCKergic cell reporter due to its preferential
357 labeling neuronal somata via cytosolic Cre. As shown by Fig 1A & 1B, the OB
358 superficial EPL and IPL were intensely labeled by tdTomato three weeks after virus
359 injection. At higher magnification, dTTCs (Fig 1C), mTCs (Fig 1D), and sTCs in the EPL

360 (Fig 1E) were easily identifiable and quantified purely based on their soma location in
361 the EPL. However, the distinguishment between sTCs and eTCs at the boundary
362 between the EPL and glomerular layer (GL) was challenging due to the lack of solid
363 criteria in the literature. To circumvent this, we established the following three
364 morphological criteria for categorization and quantification of them. (1) Soma size:
365 compared to sTCs (>15 μm diameter), eTCs have relatively small somas (<15 μm
366 diameter). (2) Length of the initial unbranched apical dendrite: sTCs have relative long
367 apical dendrites with branches distal to the soma while eTCs have short apical
368 dendrites with branches proximal to the soma. By measuring from the soma center to
369 the first branch: sTC (>30 μm) and eTC (<30 μm). (3) Soma shape and presence or
370 absence of lateral dendrites: eTCs have pear shaped somas with a round and smooth
371 base but no lateral dendrites while sTCs have lateral dendrites or protuberance(s) on
372 the somatic base even when the lateral dendrites are truncated during slicing. Thus, we
373 classified those with relatively large soma and long unbranched initial apical dendrites
374 but with protuberances at the soma base as sTC as shown in Fig 1E. Based on these
375 classification criteria, our analysis of data from OB sections collected from 3 mice
376 showed that a vast majority (82.7%) of labeled cells were sTCs (248/300 cells), 8%
377 (24/300 cells) eTCs, 4.3% (13/300 cells) mTCs, and 5% (15/300 cells) dTCs (Fig 1F).
378 This suggests that our approaches for labeling, opto- and chemogenetic manipulations
379 preferentially target CCKergic STCs.

380 **Contribution of AMPA and NMDA receptor activation to the ON-evoked STC** 381 **responses**

382 Our previous study showed that the ON-evoked responses in CCKergic STCs
383 were completely blocked the mixture of selective AMPA receptor blocker NBQX and
384 NMDA receptor blocker APV. However, the relative contribution of each receptor type is
385 unknown. To address this question, we conducted both voltage and current clamp
386 recordings of ON-evoked responses in CCKergic STCs in OB slices prepared from
387 CCK-Cre mice (Fig 2A). CCKergic STCs were identified for recording by their cell body
388 location in the superficial EPL and expression of ChR2-EYFP (Fig 2B). Consistent with
389 our previous study, electrical ON stimulation elicited excitatory postsynaptic currents
390 (EPSCs, Fig 2C black trace) or a burst of action potentials (Fig 2D black trace) in the
391 recorded STCs when they were voltage clamped at -60 mV or in current clamp and
392 perfused with normal ACSF. The duration of these responses was significantly reduced
393 by the selective NMDA receptor blocker D-APV (50 μ M, Fig 2C & 2D red traces). The
394 response charge (time integral) of ON-evoked EPSCs was decreased by 57.6% from
395 13.59 ± 2.38 pA·s to 5.76 ± 1.06 pA·s ($n=5$ cells, $t_{(8)}= 4.33427$, $p=0.00749$,
396 ANOVAOneWayRM with Bonferroni comparison) (Fig 2E) while EPSC amplitude was
397 not significantly changed by D-APV with 74.1 ± 10.6 pA in ACSF vs 61.3 ± 8.8 pA in D-
398 APV ($n=5$ cells, $t_{(8)}= 1.55357$, $p=0.45401$, ANOVAOneWayRM with Bonferroni
399 comparison) (Fig 2F). Congruently, the ON-evoked burst duration, the peak time stamp
400 difference between the first and last action potentials, was reduced by 54% from
401 241.4 ± 35.5 ms to 110.9 ± 22.5 ms ($n=5$ cells, $t_{(8)}= 4.01954$, $p=0.01153$,
402 ANOVAOneWayRM with Bonferroni comparison) whereas the number of action
403 potentials (APs)/response decreased by 39.7% from 9.04 ± 0.89 to 5.45 ± 1.07 ($n=5$ cells,
404 $t_{(8)}= 3.86459$, $p=0.01433$, ANOVAOneWayRM with Bonferroni comparison). The

405 residual components of ON-evoked responses were completely blocked by the
406 combination of selective AMPA and NMDA receptor blockers DNQX (20 μ M) and D-
407 APV (50 μ M) (Fig 2C-2H). These findings demonstrate that NMDA receptors in STCs
408 actively participate and amplify the ON-elicited postsynaptic responses.

409 **STCs provide excitatory feed forward Input to Mitral Cells via their Apical**

410 **Dendrites**

411 Previous studies demonstrate that single apical dendrites of STCs ramify in
412 individual glomeruli (Orona et al., 1984; Liu and Shipley, 1994; Sun et al., 2020) where
413 they potentially establish synaptic connections with local interneurons and/or apical
414 dendrites of mitral/tufted cells. Actually, STCs form dendro-dendritic synapses with two
415 populations of GABAergic interneurons short axon cells (SACs) and periglomerular cells
416 (PGCs), highlighting a role of STCs in coordinating inhibitory circuits in the glomerular
417 layer (Sun et al. 2020). A recent study reported that optogenetic silencing of CCKergic
418 cells can reduce MC excitatory responses evoked by OSN stimulation (Zak and
419 Schoppa, 2021), indicating the participation of CCKergic neurons in the ON-evoked MC
420 output. However, direct evidence supporting the CCKergic TC→MC transmission is
421 lacking. To examine potential dendro-dendritic synaptic transmission from STCs to MCs
422 in the glomerulus, recordings were made from MCs on the medial side of OB slices
423 prepared from CCK-Cre mice with ChR2 expression in CCKergic STCs as shown in Fig
424 2A. Alexa fluor 594 (10 μ M) was included in the internal solution to visualize MC apical
425 dendrites thus guiding the delivery of LED blue light (470 nm) to the targeted glomerulus
426 for optogenetic activation of CCKergic STC apical dendrites (Fig 3A). The circular area
427 of blue light (~50-90 μ m in diameter) was configured and generated by a Polygon 400E

428 and presented through the microscopic objective lens to activate ChR2 expressed on
429 CCKergic STC apical dendrites. Brief (1 ms) optical stimulation reliably (20/20 traces in
430 each cell) evoked long-lasting inward currents in the recorded MCs (Fig 3B). These
431 responses were characterized by a short onset-latency (figure 3C) and predominately
432 mediated by NMDARs as application of APV dramatically reduced the response charge
433 by 94.2% from 190.97 ± 33.8 pA·s to 11.05 ± 1.86 pA·s ($n=7$ cells, $t_{(12)}= 6.58893$,
434 $p<0.0001$, ANOVAOneWayRM with Bonferroni comparison) but not the amplitude of the
435 inward current, which was 167.2 ± 19.9 pA in ACSF and 138.0 ± 19.6 pA ($n=7$ cells, $t_{(12)}=$
436 1.7478 , $p=0.31804$, ANOVAOneWayRM with Bonferroni comparison) (Fig 3B, 3D & 3E).
437 These long-lasting responses have consistently short onset latencies (2.0 ± 0.1 ms, $n=7$
438 cells) with an average jitter at 279.3 ± 48.8 ms, indicating a dendrodendritic
439 monosynaptic transmission from STCs to MCs. Due to the relatively long jitter value and
440 potential confound effects of strong optogenetic stimulation, glutamate spill-over may
441 also contribute to this response as previously reported in eTCs (Gire et al., 2019).
442 Addition of DNQX significantly decreased the response charge and amplitude of the
443 optical stimulation-evoked brief inward current in the presence of APV (Fig 3B, 3D & 3E)
444 but with a small residual inward current with an average charge at $1.75 \pm .49$ pA·s ($n=7$
445 cells, $t_{(12)}= 0.3404$, $p=1$ compared to APV but $t_{(12)}= 6.92933$, $p<0.0001$ compared to
446 ACSF, ANOVAOneWayRM with Bonferroni comparison) and amplitude at 39.0 ± 9.0 pA
447 ($n=7$ cells, $t_{(12)}= 5.94059$, $p=0.000204353$ compared to APV and $t_{(12)}= 7.68839$,
448 $p<0.0001$ compared to ACSF, ANOVAOneWayRM with Bonferroni comparison) (Fig 3B
449 green trace, 3D & 3E), indicating that AMPA receptors mediate vast majority of these
450 brief responses. Likewise, the same optical stimulation in current clamp reliably evoked

451 long-lasting depolarization (LLD) superimposed by bursts of APs (Fig 3F), which have
452 an averaged spikes/response in 5 cells at 43.4 ± 13.2 and burst duration at 1507.1 ± 461.7
453 ms in ACSF. These values were respectively reduced by bath-applied APV by 91.5% to
454 3.7 ± 0.9 (Fig 3G, $n=5$, $t_{(8)}= 3.6707$, $p=0.01891$ compared to ACSF, ANOVAOneWayRM
455 with Bonferroni comparison) and by 96.8% to 48.8 ± 13.7 ms (Fig 3H, $n=5$, $t_{(8)}= 3.87493$,
456 $p=0.01413$ compared to ACSF, ANOVAOneWayRM with Bonferroni comparison)
457 whereas addition of DNQX abolished all the remaining evoked spikes (Fig 3F-3H).
458 Collectively, these findings establish that apical dendrites of STCs and MCs form
459 glutamatergic connections in the glomerulus where STCs provide robust feedforward
460 excitation to reliably evoke LLDs in MCs. These STC-evoked responses are
461 predominantly mediated by activation of postsynaptic NMDARs and AMPARs in MCs.

462 **STCs amplify the ON input-evoked mitral cell responses**

463 Since CCKergic STCs respond to single ON-stimulation with a burst of action
464 potentials (Fig 2) (Jones et al., 2020; Sun et al., 2020) and intermediate long-lasting
465 feedforward excitation to MCs (Fig 3) forming the ON→STC→MC pathway, we predict
466 that CCKergic STCs amplify MC output in response to ON input. To test this, we
467 expressed halorhodopsin (eNpHR) in CCKergic STCs by injecting the Cre-dependent
468 AAV5-Ef1 α -DIO-eNpHR 3.0-EYFP (AAV-HR-YFP) into the medial side of each OB of
469 CCK-Cre mice. Similar to ChR2-EYFP expression (Fig 2A), eNpHR-EYFP was
470 predominately expressed in the superficial EPL, GL, and IPL, respectively,
471 corresponding to the location of CCK-TC somata, apical dendrites and axonal
472 projections/terminations (Fig 4A). This distribution of EYFP expression was consistent
473 with the previously reported CCK expression in the OB (Seroogy et al., 1985; Liu and

474 Shipley, 1994; Sun et al., 2020), highlighting preferential eNpHR expression in CCK-
475 containing STCs in the OB. To verify eNpHR functionality, EYFP-expressing neurons in
476 OB slices were recorded in the presence of APV (50 μ M), DNQX (20 μ M), and the
477 selective GABA_A receptor blocker gabazine (10 μ M). A circular green LED light (~20 μ M
478 in diameter) was delivered to stimulate only the cell body of the recorded YFP-
479 expressing cells. A 200 ms or 2 s green light (590 nm) stimulation reliably evoked
480 outward currents or complete termination of spontaneous firing activities and membrane
481 hyperpolarization, which lasted for the whole duration of light exposure, in all recorded
482 cells (n=5) that were voltage clamped at -60 mV or in current clamp, respectively (Fig
483 4B). No responses were observed from EYFP negative cells on the same side or on the
484 opposite side of the bulb (Data not shown). These findings validated the effectiveness of
485 our optogenetic approach for selective labeling and inhibiting STCs. To ensure
486 consistency and comparability, we used the same level of light stimulation power for all
487 remaining optogenetic experiments. To test whether CCKergic STCs play a role in
488 amplifying the ON-evoked responses in MCs, we recorded MCs in current clamp while
489 ON electrical stimulation and green light optical stimulation were delivered to ON layer
490 and the glomeruli receiving apical dendrites of the recorded MCs, respectively (Fig 5A).
491 As shown in Fig 5B, ON stimulation elicited a burst of action potentials in a typically
492 recorded MC (top trace). When the green light was on, the membrane potential was
493 hyperpolarized in the recorded MCs during the whole period of light exposure (Fig 5B
494 middle and bottom traces). However, the same ON stimulation applied in the presence
495 of green light exposure evoked no action potentials in the recorded MC (Fig 5B middle
496 and bottom traces). These findings were replicated in all recorded MCs (n=7, Fig 5C &

497 5D). Specifically, ON-evoked burst duration and number of action potentials were
498 reduced from 616.6 ± 98.8 ms and 16.9 ± 1.3 in control to 5.9 ± 3.9 ms ($n=7$, $p < 0.0001$,
499 paired t -test) and 0.5 ± 0.3 ($n=7$, $p < 0.00001$, paired t -test) during green light exposure,
500 respectively (Fig 5C & 5D). This significantly reduced MC response to ON stimulation in
501 the presence of green light exposure to CCKergic STCs likely reflects optogenetic
502 inhibition of the CCKergic STC-mediated feedforward excitation to MCs. Moreover,
503 green light produced hyperpolarization of MCs could also contribute to this effect.

504 **Gap junction contributes to the STC→MC transmission**

505 To differentiate these possibilities, we first tested whether optogenetic inhibition
506 of CCKergic STCs hyperpolarized MCs. Although CCKergic STCs via their apical
507 dendrites drive MCs (Fig 3) and GABAergic interneurons in the glomerular layer (Sun et
508 al., 2020) which provide forward inhibition to MCs (Shao et al., 2009; Shao et al., 2012;
509 Banerjee et al., 2015; Liu et al., 2016; Burton, 2017), selective inhibition of this
510 subpopulation of excitatory tufted cells is not predicted to hyperpolarization of MCs
511 unless there is a tonic excitatory driving of MCs by the CCKergic STCs or a gap junction
512 between STCs and MCs. But the first possibility is not supported by our finding of the
513 synaptic blocker-resistant excitation in MCs by optogenetic activation of CCKergic STCs
514 (Fig 3B and 3F green traces). Thus, we hypothesized the existence of gap junction-
515 mediated electrical synapses between STCs and MCs. To test this idea, we voltage
516 clamped MCs at -60 mV in the presence of glutamatergic synaptic blockers DNQX (10
517 μ M) and APV (50 μ M) and compared their responses to either optogenetic excitation or
518 inhibition of CCKergic STCs before and after bath application of the gap junction blocker
519 carbenoxolone (CBX, 300 μ M). As shown in Fig 6A and 6B, the MC responded with an

520 inward current to blue light stimulation of the glomerulus receiving apical dendrite of the
521 recorded MCs in OB slices prepared from CCK-Cre mouse with ChR2-EYFP expression
522 in the CCKergic STCs. This response was completely eliminated by CBX treatment for
523 10 min. Specifically, the charge of this current in 6 MCs was reduced from 2.11 ± 0.25
524 pA·s to 0.006 ± 0.001 pA·s ($n=6$ cells, $p < 0.0001$ paired t -test) by CBX (Fig 6B & 6E),
525 indicating a gap junction-mediated transmission from STCs to MCs in the glomerulus.

526 In a separate set of experiments, MCs were voltage clamped at -60 mV in OB
527 slices prepared from CCK-Cre mice with eNpHR expression in CCKergic STCs in the
528 presence of DNQX and APV to block excitatory synaptic activities. When green light
529 was presented to the glomeruli targeted by the apical dendrites of the recorded MCs to
530 inhibit CCKergic STCs (Fig 6C), robust outward currents were recorded in 6/9 MCs (Fig
531 6D). These outward currents lasted for the whole period of green light exposure but
532 were followed by long-lasting inward currents once the light stimulation was turned off.
533 These green light-evoked inward and outward currents were abolished by CBX (Fig 6D
534 & 6F). The average charge of these outward and inward currents was respectively
535 reduced from 10.5 ± 1.2 pA·s and 13.8 ± 1.6 pA·s to 0.3 ± 0.2 pA·s ($n=6$ cell, $p < 0.0001$,
536 paired t -test) and 0.5 ± 0.1 pA·s ($n=6$ cell, $p < 0.0001$, paired t -test) after bath application
537 of CBX for 10 min (Fig 6F). To test whether the intracellular dialysis-caused rundown via
538 the patch pipette solution contributes to the observed CBX effects, we performed
539 another set of recordings without CBX treatment as control. The comparison of these
540 inward and outward currents between without and without CBX treatment ruled out this
541 possibility (Fig 6F). Taken together, these results demonstrating the complete
542 elimination of bidirectional responses in MCs in response to optogenetic excitation or

543 inhibition of CCKergic STCs by CBX strongly support gap junction-mediated electrical
544 synapses formed between the apical dendrites of STCs and MCs in the glomerulus.

545 To reassess STC role in intermediating ON-elicited MC responses by eliminating
546 confound influences from gap junctions, we recorded MCs in current clamp while ON
547 stimulation was delivered to the ONL in the presence of the gap junction blocker CBX
548 (Fig 7A). Consistent with voltage clamp results, MCs no longer responded to green light
549 stimulation with hyperpolarization after OB slices were perfused with 300 μ M CBX for
550 10 min (data not shown). In the presence of CBX, ON stimulation evoked a long burst of
551 action potentials in MCs (Fig 7B). However, MCs responded to the same ON stimulation
552 with only a depolarization (EPSP) with fewer or no superimposed action potentials when
553 the green light stimulation was turned on to selectively inhibit the CCKergic STCs
554 affiliated with the glomeruli receiving apical dendrites of the recorded MCs (Fig 7B-7D).
555 On the average of 5 cells, the ON-evoked number of action potentials (Fig 7C) and
556 burst duration (Fig 7D) were reduced from 10.6 ± 1.1 and 279.2 ± 47.0 ms in the presence
557 of CBX to 2.6 ± 0.1 (n=5 cells, $p < 0.005$ paired *t*-Test) and 36.1 ± 7.9 ms (n=5 cells,
558 $p < 0.005$ paired *t*-Test) in the presence of both CBX and green light stimulation,
559 respectively. These results support the role of the CCKergic STCs in amplifying MC
560 output to ON-input in the absence of gap junction.

561 In summary, these studies demonstrate that STCs provide a robust feed-forward
562 excitation to MCs via both chemical and electrical connections formed between the STC
563 and MC apical dendrites and amplify OB output to downstream centers in response to
564 ON stimulation.

565 **Stimulation of CCKergic STC axons excites MCs on the opposite side of the OB**

566 STC axons project to the IPL where they turn abruptly to course ventrally and
567 dorsally to terminate in the IPL right beneath the mirror glomerulus on the opposite side
568 of the same bulb (Liu and Shipley, 1994; Belluscio et al., 2002; Lodovichi et al., 2003;
569 Igarashi et al., 2012). Previous studies have demonstrated that axon terminals of the
570 CCKergic STCs provide monosynaptic inputs to GCs on the opposite side of the same
571 OB (Liu and Shipley, 1994; Sun et al., 2020). However, whether there are functional
572 connections formed between STC axon terminals and axon collaterals or somata of
573 local MCs on the opposite side of the same bulb remains unknown. To answer this
574 question, we injected 100 nl AAV into the EPL of the OB medial side of CCK-Cre mice
575 to confine ChR2-mCherry expression only in local CCKergic STCs but not in those on
576 the opposite side (Fig 8A). In OB slices prepared from these animals, voltage clamp
577 recordings were made from MCs on the lateral side of the OB where ChR2-mCherry
578 expression was detected only in the IPL but not in the superficial EPL or glomerular
579 layer (Fig 8A). To visualize the recorded cells and their apical dendrites, Alexa Fluor
580 594 (10 μ M) was included in the recording patch pipette. No ChR2 expression in
581 CCKergic tufted cells on the later side was further functionally verified by presenting the
582 blue light to the glomeruli receiving the apical dendrites of the recorded cells (Fig 8A). In
583 these conditions, inward currents with a brief and large amplitude component followed
584 by a slow and small amplitude component were recorded in all 5 MCs in response to a
585 small sized (30 μ m diameter) blue light delivered to the IPL right below the recorded
586 cells (Fig 8C) but not by a large sized (90 μ m diameter) blue light presented to the
587 glomeruli receiving their apical dendrites (Fig 8A & 8B). This was an unexpected
588 observation as no prior evidence indicates this. To further preclude potential synaptic

589 contribution from apical dendrites in the glomeruli of the recorded cells, 3 MCs with
590 apical dendrites truncated during slice preparation (Fig 8B) were selected for recording
591 but showed similar responses to optical stimulation delivered to the IPL right below
592 somata of the recorded cells. Bath-applied APV (100 μ M) completely eliminated the
593 slow and small component of the response but only slightly reduced the amplitude of
594 the brief component, which was significantly reduced by addition of 20 μ M DNQX. Due
595 to no significant differences of their responses, data from the cells with intact or
596 truncated apical dendrites were pooled together for analysis. The averaged charge of
597 the whole response (Fig 8D) and amplitude of the brief EPSC (Fig 8E) in 8 MCs were
598 12.11 ± 4.48 pA·s and 20.5 ± 2.3 pA in ACSF, 2.96 ± 0.84 pA·ms ($t_{(14)}=2.7193$, $p=0.04985$
599 compared to ACSF, ANOVARM) and 17.4 ± 2.6 pA ($t_{(14)}= 1.38977$, $p=0.55892$ compared
600 to ACSF, ANOVARM) in APV, and 0.21 ± 0.07 pA·s ($t_{(14)}= 0.81741$, $p=1$ compared to
601 APV; $t_{(14)}= 3.53671$, $p=0.00986$ compared to ACSF, ANOVARM) and 4.1 ± 1.40 pA
602 ($t_{(14)}= 5.79907$, $p=0.00013812$ compared to APV; $t_{(14)}= 7.18884$, $p<0.0001$ compared to
603 ACSF, ANOVARM) in APV+DNQX, respectively. These results suggest a glutamatergic
604 transmission from the CCKergic STC axons to MCs in the IPL on the opposite side of
605 the same OB. However, the averaged onset latency of these responses in 8 cells was
606 4.7 ± 0.6 ms with a jitter at 1088.7 ± 208.1 μ s (Fig 8F). Taken together, the results of this
607 experiment revealed a CCKergic STC-provided feedforward excitation to MCs on the
608 opposite side of the same bulb, which is potentially polysynaptic or mediated by
609 glutamate spillover.

610 **CCKergic STCs function to increase olfactory sensitivity**

611 The capacity for STCs to mediate MC responses to ON input via dendrodendritic
612 transmission in the glomerulus and simultaneously excite MCs on the opposite side of
613 the same OB in the IPL led us to hypothesize that IAS-STCs amplify MC output in response
614 to sensory input thus function to regulate the system's sensitivity to odorant stimuli. To
615 test this, we compared animal's sensitivity to odorants by two sets of behavioral tests
616 among CCK-Cre mice that are randomly assigned to two groups with expression of
617 either the inhibitory DREADD hMD₄G_i or ChR2 in the OB CCKergic STCs. Animals in
618 each group was further divided into two subgroups with intraperitoneal (i.p.) injection of
619 either the hMD₄G_i actuator clozapine-N-oxide (CNO) to activate the inhibitory DREADD
620 in CCKergic STCs or saline 30 min before behavioral tests. Since saline does not
621 activate hMD₄G_i and neither CNO nor saline activates ChR2, CCKergic STCs were
622 chemogenetically inhibited only in mice with hMD₄G_i expression and i.p. injection of
623 CNO while mice in the other three groups including hMD₄G_i/saline, ChR2/CNO, and
624 ChR2/saline, served as control animals. Thus, the comparison of behavioral
625 performance was made among the following four groups of CCK-Cre mice to determine
626 the functional roles of STCs: (1) AAV5-hMD₄G_i-mCherry injection in the OB with CNO
627 injection (DREADD/CNO), (2) same virus injection as in (1) but with saline injection
628 (DREADD/saline), (3) AAV5-ChR2-mCherry injection in the OB with CNO injection
629 (ChR2/CNO), (4) same virus injection but with saline injection (ChR2/saline). As shown
630 in figure 9A, the DREADD-mCherry was consistently expressed in the OB 3 weeks after
631 virus injection with an expression pattern similar to that of ChR2 or HR. Bath-applied
632 CNO (10 μ M) hyperpolarized and terminated spontaneous action potentials in all
633 recorded hMD₄G_i-mCherry-expressing neurons (5/5 cells) in OB slices (Fig 9B-9D) but

634 not in the Chr2-mCherry expressing cells (n=6 cells, data not shown). Specifically, the
635 spontaneous firing rate was reduced from 70.0 ± 4.7 Hz in control to 2.7 ± 1.0 Hz by CNO
636 treatment (n=5 cells, $t_{(4)}=16.04017$, $p < 0.0001$, paired *t* test) where the membrane
637 potential was changed from -57.3 ± 2.8 mV to -61.8 ± 1.9 mV (n=5, $t_{(4)}=4.03587$,
638 $p=0.01566$, paired *t* test) by bath application of CNO. These results corroborate the
639 effectiveness of our chemogenetic approach on inhibiting the CCKergic STCs.

640 To investigate the functional role of OB CCKergic STCs in regulating animal's
641 sensitivity to odorant stimuli, we conducted the buried food test (Yang and Crawley,
642 2009; Machado et al., 2018), a behavioral assay for assessing olfactory detection.
643 Three weeks after the injection of AAV5-hMD4Gi-mCherry or AAV-ChR2-mCherry (200
644 nl/site) into both the medial and later side of each OB, animals were subject to 23-hour
645 food deprivation before performing the behavioral test (Fig 10A). As shown in figure
646 10B, the latency (126.2 ± 61.9 s, n=19) for the group of DREADD/CNO mice to identify
647 the buried food was significantly longer than that of the other three groups, which is
648 59.8 ± 13.7 s (n=16, $t=3.27579$, $p=0.01015$ compared to DREADD/CNO,
649 ANOVATwoWay) for the DREADD/saline group, 61.9 ± 10.1 s (n=18, $t=3.27362$,
650 $p=0.01022$ compared to DREADD/CNO, ANOVATwoWay) for the Chr2/CNO group,
651 and 55.7 ± 11.3 s (n=16, $t=3.4793$, $p=0.00542$ compared to DREADD/CNO,
652 ANOVATwoWay) for the Chr2/saline group. By contrast, there was no difference in the
653 latencies for animals to locate the food pellets placed on the surface of bedding material
654 (Fig 10C), indicating no contribution of visual or motor disability to the difference in
655 buried food test results. Consistently, difference among the four groups of mice was
656 detected in neither the total traveling distance (Fig 10D) nor traveling distance in the

657 center of open field test arena (Fig 10E) in the open field test, suggesting that functional
658 inhibition of the CCKergic STCs via the chemogenetic approach does not affect
659 animal's general motor function or anxiety level. Collectively, these behavioral outcomes
660 strongly suggest that the CCKergic STCs function to regulate the animal's sensitivity to
661 odor detection.

662 Next, we measured olfactory detection threshold using a two-bottle discrimination
663 assay (Wysocki et al., 1977; Pourtier and Sicard, 1990; Griff and Reed, 1995), in which
664 animals had a choice of drinking from two water bottles: one non-odorized and the other
665 odorized by the monomolecular odorant isovaleric acid (iVA) at decreasing
666 concentrations (Fig 11A). Since iVA is conditioned by a single dose of i.p. injection of
667 lithium chloride (LiCl) that produces nausea-related behaviors and symptoms consistent
668 with visceral illness in non-emetic species including mice (Ossenkopp and Eckel, 1995;
669 Hanak et al., 2017), animals preferentially avoid drinking from the iVA-odorized water
670 bottle until the iVA concentration decreases to or below the detection threshold. In order
671 to motivate animals to drink from the odorized water and facilitate the LiCl-induced
672 aversion, animals were subject to 23 hours water deprivation before the test (Fig 11A).
673 The results are presented as a preference index of the odorized water for each group of
674 animals (n=13 mice/group), which was calculated as the amount of the odorized water
675 consumed divided by the total amount of liquid consumed (both odorized water and no-
676 odorized water) daily. Since the random chance to drink from each bottle is 50%, the
677 highest concentration of iVA is interpreted as the animal's detection threshold once its
678 preferential index is not statistically significant from 0.5. As shown in Fig 11B, the iVA
679 preferential indexes for three groups of control mice reached 50% after iVA

680 concentration was decreased to 10^{-6} or 10^{-7} M, indicating their detection threshold is
681 about 10^{-6} M. However, the iVA preferential index of the DREADD/CNO group of mice in
682 the concentration range from 10^{-5} M to 10^{-3} M was significantly lower than that in each
683 of the other three groups (one-way ANOVA analysis, Fig 11B), suggesting that
684 chemogenetic inhibition of the CCKergic STCs significantly elevates the animal's
685 detection threshold for iVA compared to control mice. Taken together, these findings
686 strongly support the important roles of CCKergic STCs in amplifying odorant signals to
687 MCs thus enhancing the system's sensitivity to odorants.

688 **DISCUSSION**

689 Five major findings were generated from the present study focusing on how
690 functional modulation of CCKergic STCs, the predominant structural elements of the
691 IAS, with optogenetic and chemogenetic approaches impacts the physiological output of
692 MCs in the OB and the odor-based behavioral outcomes. First, both AMPA and NMDA
693 receptors contributes to the ON-evoked monosynaptic responses in the CCKergic
694 STCs. NMDA receptors mediates the long-lasting and late component of these events.
695 Second, CCKergic STCs provide long-lasting synaptic excitation to MCs via
696 dendrodendritic transmission in the glomerulus. This STC→MC transmission is
697 mediated by both glutamate-mediated chemical and gap junction-based electrical
698 synapses. Third, excitatory STC input significantly amplifies MC output in responses to
699 ON stimulation. Fourth, axons from the CCKergic STCs on the opposite side of the
700 same OB provide excitatory feedforward to local MCs. Lastly, functional inhibition of
701 CCKergic STCs impairs odor detection by drastic reduction of animal's sensitivity to
702 odors.

703 Based on ultrastructural evidence of synaptic connections between CCKergic TC
704 axons and GC dendrites in the IPL, the IAS was initially proposed to function as a
705 neural circuit linking the infraglomerular inhibitory circuits on the medial and lateral sides
706 of the same bulb (Liu and Shipley, 1994). The functional operation of this axodendritic
707 STC→GC synapse was recently characterized (Sun et al., 2020). Moreover, CCKergic
708 STCs drive two subpopulations of inhibitory glomerular interneurons via their apical
709 dendrites. Intriguingly, among these inhibitory glomerular interneurons and GCs, only
710 the short axon cells (SACs) can be activated by CCK at a physiological concentration
711 (Liu and Liu, 2018), suggesting the SAC-mediated lateral inhibition in the OB can be
712 further elevated by endogenous CCK potentially released from CCKergic STCs when
713 they fire high frequency action potentials in response to repetitive OSN input (Ghijzen et
714 al., 2001; Jones et al., 2020; Sun et al., 2020). All these experimental findings suggest
715 that CCKergic STCs form the IAS and recruit different inhibitory circuits to process odor
716 information in the OB (Fig 12A).

717 In contrast to their dynamic actions on inhibitory circuits, the present study for the
718 first time provided multiple lines of evidence supporting that CCKergic STCs play a
719 functionally amplifying role in transforming the OB input to output and enabling the
720 system to detect weak odorant stimuli from the environment via their synaptic
721 connections with MCs at multiple levels (Fig 12A).

722 First, activation of NMDA receptors significantly augments STC output in
723 response to monosynaptic OSN input. This finding aligns with previous studies showing
724 that STCs respond to OSN input in OB slices or odorants especially at low
725 concentration in whole animals with more reliable responses of larger amplitude and

726 shorter latencies or more spikes compared to MCs (Griff et al., 2008; Short and
727 Wachowiak, 2019; Eiting and Wachowiak, 2020; Jones et al., 2020). Although the
728 relatively high input resistance and small soma sizes potentially contribute to the strong
729 CCKergic STC response to OSN input (Jones et al., 2020), the present study provides
730 the pharmacological evidence supporting the contribution of NMDA receptors to
731 enabling the CCKergic STCs to respond to weak odor stimuli.

732 Second, CCKergic STCs excite MCs in the glomerulus via dendrodendritic
733 chemical transmission and electrical synapses. Optogenetic activation of CCKergic STC
734 apical dendrites elicited a long-lasting inward current or a long train of action potentials
735 in MCs with apical dendrites affiliated with the activated glomerulus. Since CCKergic
736 STCs exclusively receive monosynaptic OSN input (Jones et al., 2020; Sun et al.,
737 2020), this finding implies contribution of CCKergic STCs to the ON-evoked long-lasting
738 depolarization in MCs (Carlson et al., 2000) like the external tufted cells (ETCs) (De
739 Saint Jan et al., 2009; Najac et al., 2011; Gire et al., 2012), a distinct subpopulation of
740 TCs with somata confined to the glomerular layer but lacking lateral dendrites (Macrides
741 and Schneider, 1982; Hayar et al., 2004; Antal et al., 2006). This conclusion is further
742 supported by the observation that the ON-evoked MC responses were significantly
743 reduced by optogenetic inhibition of CCKergic STCs. The STC→MC dendrodendritic
744 transmission qualitatively aligns with a previous study (Zhou and Belluscio, 2008).
745 Dendrodendritic synapses between excitatory neurons in the glomerulus were identified
746 or indicated in previous ultrastructural studies (Hinds, 1970; Kosaka and Kosaka, 2005;
747 Bourne and Schoppa, 2017). However, due to their rarity, we cannot rule out the
748 possibility that the STC→MC responses observed here could be mainly mediated by

749 glutamate spillover, despite their short latencies, which may result from strong
750 optogenetic stimulation of the presynaptic neurons (Gire et al., 2019). Nevertheless,
751 NMDA receptors on MCs play a crucial role in enhancing MC responses to CCKergic
752 STC input via dendrodendritic transmission within the glomerulus.

753 In addition to the glutamate-mediated transmission, gap junction contributes to a
754 nonnegligible portion (~23% of initial EPSC amplitude) of the STC-evoked excitatory
755 response in MCs. This observation is consistent with previous work showing gap
756 junctions between intraglomerular MTC dendrites (Kosaka and Kosaka, 2004) and
757 similar to that observed in the ETC-MC connection (Gire et al., 2012). In addition to
758 boosting the glutamate-mediated transmission from STCs to MCs, this electrical
759 synapse could also play a role in synchronize activities between STCs and MCs in the
760 glomerulus and/or produce a shunting effect between them but to a less extent
761 compared to MC-MC gap junction (Christie et al., 2005).

762 Third, STCs activate MCs on the opposite side of the same bulb via their axons
763 traveling within the IPL. Different from the dendrodendritic transmission between the
764 apical dendrites of CCKergic STCs and MCs in the glomerulus, the glutamate-mediated
765 MC response to optogenetic activation of axons in the IPL projecting from CCKergic
766 STCs on the opposite side of the OB was mainly mediated by AMPA receptors but
767 showed a relatively long onset latency (~5 ms). Considering the existence of many
768 experimental variables such as the level of ChR2 expression on axon terminals of
769 CCKergic STCs and the depth of the activated axons from the slice surface leading to
770 temporally differential levels of glutamate release, the relative long onset latency of MC
771 response in this context does not exclude the possible monosynaptic nature of this

772 transmission. Furthermore, there were two cells (one with an intact apical dendrite and
773 other with truncated apical dendrite) showed short latencies (2.6 ± 0.1 ms) and small jitter
774 ($410.5 \mu\text{s}$) (Fig 8F), consistent with monosynaptic transmission. Intriguingly, a previous
775 study reported similar response latencies in MCs when the electrical stimulation was
776 given to the IPL on the opposite side under the mirror glomerulus to antidromically
777 activate the IAS-forming TCs with apical dendrites ramifying in the same glomerulus of
778 the recorded MC in a hemibulb slice preparation (Zhou and Belluscio, 2008). In that
779 scenario, the transmission should be monosynaptic between the apical dendrites of TCs
780 and MCs. Additionally, the lack of excitatory interneurons in the IPL does not support
781 polysynaptic transmission from CCKergic TC axons to MCs. Whether this is a spillover
782 action of glutamate released from CCKergic axon terminals in the IPL is worth future
783 work.

784 The functional significance of STC-MC connections in the IPL on the opposite
785 side of the same OB can be speculated to involve synchronizing MC output from mirror
786 glomeruli based on previous evidence showing that IAS axons terminate precisely
787 beneath mirror glomeruli on the opposite OB side (Belluscio et al., 2002; Lodovichi et
788 al., 2003; Zhou and Belluscio, 2008). However, our study does not provide direct
789 evidence for this hypothesis. Additionally, other possibilities cannot be ruled out, such
790 as the activation of MCs associated with neighboring glomeruli, particularly given the
791 potential branching of STC axons in the IPL (Orona et al., 1984). Alternatively, STC-MC
792 excitation could be counterbalanced by inhibition from local granule cells, which also
793 receive STC axonal input in the IPL (Liu and Shipley, 1994; Sun et al., 2020). This
794 inhibitory influence may be further modulated by strong excitatory input from cortical

795 centrifugal projections, such as those from the piriform cortex (Boyd et al., 2012) or the
796 anterior olfactory nucleus (Markopoulos et al., 2012). Therefore, whether the net
797 functional impact of this circuit on MC output from mirror or relevant glomeruli is
798 excitatory or inhibitory depends on the interplay between MC-derived excitation and
799 GC-mediated inhibition.

800 Finally, animal's sensitivity to food odor and iVA was significantly reduced by
801 chemogenetic inhibition of the CCKergic STCs. Although STC axons project out of
802 the OB to target the anterior piriform cortex (APC), the par externa of the anterior
803 olfactory nucleus (AON), and the cap part of the olfactory tubercle (OT) (Igarashi et al.,
804 2012; Hirata, 2024) could contribute to these effects because these downstream
805 structures may play a role in olfactory perception, odor detection or discrimination, but a
806 straightforward speculation based on findings of the present study is that CCKergic
807 STCs regulate the system's sensitivity to odor stimuli by acting on MCs affiliated with
808 mirror glomeruli via the IAS (Fig 12B).

809 Taken together, the present study demonstrated glutamatergic excitation of MCs
810 on the medial and lateral sides of the same bulb by the CCKergic STCs. This excitatory
811 feedforward connection could be particularly important for the system to detect weak
812 odor stimuli as we speculate that the simultaneous excitation from the STCs affiliated
813 with mirror glomeruli on both sides of the OB will summate to boost the weak
814 stimulation-produced subthreshold MC responses to the suprathreshold level leading to
815 spike output to downstream centers (Fig 12B). Given that temporal integration of
816 convergent OB output from multiple glomeruli determines the firing probability of
817 pyramidal neurons in the piriform cortex (Zhou and Belluscio, 2008; Apicella et al.,

818 2010), we further speculate that CCKergic STCs function to ensure weak odor detection
819 and representation in the cortex by amplifying and synchronizing MC output from mirror
820 glomeruli. These speculations certainly necessitate future research endeavor.

821 References

822

823 **Uncategorized References**

- 824 Allen DC, Carlson TL, Xiong Y, Jin J, Grant KA, Cuzon Carlson VC (2019) A
825 Comparative Study of the Pharmacokinetics of Clozapine N-Oxide and Clozapine
826 N-Oxide Hydrochloride Salt in Rhesus Macaques. *J Pharmacol Exp Ther*
827 368:199-207.
- 828 Antal M, Eyre M, Finklea B, Nusser Z (2006) External tufted cells in the main olfactory
829 bulb form two distinct subpopulations. *Eur J Neurosci* 24:1124-1136.
- 830 Apfelbach R, Russ, D. & Slotnick, B. M. (1991) Ontogenetic changes in odor sensitivity,
831 olfactory receptor area and olfactory receptor density in the rat. *Chem Senses*
832 16:10.
- 833 Apicella A, Yuan Q, Scanziani M, Isaacson JS (2010) Pyramidal cells in piriform cortex
834 receive convergent input from distinct olfactory bulb glomeruli. *J Neurosci*
835 30:14255-14260.
- 836 Banerjee A, Marbach F, Anselmi F, Koh MS, Davis MB, Garcia da Silva P, Delevich K,
837 Oyibo HK, Gupta P, Li B, Albeanu DF (2015) An Interglomerular Circuit Gates
838 Glomerular Output and Implements Gain Control in the Mouse Olfactory Bulb.
839 *Neuron* 87:193-207.
- 840 Belluscio L, Lodovichi C, Feinstein P, Mombaerts P, Katz LC (2002) Odorant receptors
841 instruct functional circuitry in the mouse olfactory bulb. *Nature* 419:296-300.
- 842 Bourne JN, Schoppa NE (2017) Three-dimensional synaptic analyses of mitral cell and
843 external tufted cell dendrites in rat olfactory bulb glomeruli. *J Comp Neurol*
844 525:592-609.
- 845 Boyd AM, Sturgill JF, Poo C, Isaacson JS (2012) Cortical feedback control of olfactory
846 bulb circuits. *Neuron* 76:1161-1174.
- 847 Buck L, Axel R (1991) A novel multigene family may encode odorant receptors: a
848 molecular basis for odor recognition. *Cell* 65:175-187.
- 849 Buck LB (1996) Information coding in the vertebrate olfactory system. *Annu Rev*
850 *Neurosci* 19:517-544.
- 851 Burton SD (2017) Inhibitory circuits of the mammalian main olfactory bulb. *J*
852 *Neurophysiol* 118:2034-2051.
- 853 Burton SD, Urban NN (2014) Greater excitability and firing irregularity of tufted cells
854 underlies distinct afferent-evoked activity of olfactory bulb mitral and tufted cells.
855 *J Physiol* 592:2097-2118.
- 856 Carlson GC, Shipley MT, Keller A (2000) Long-lasting depolarizations in mitral cells of
857 the rat olfactory bulb. *J Neurosci* 20:2011-2021.

858 Cheetham CE, Grier BD, Belluscio L (2015) Bulk regional viral injection in neonatal mice
859 enables structural and functional interrogation of defined neuronal populations
860 throughout targeted brain areas. *Front Neural Circuits* 9:72.

861 Chen F, He A, Tang Q, Li S, Liu X, Yin Z, Yao Q, Yu Y, Li A (2024) Cholecystokinin-
862 expressing superficial tufted cells modulate odour representation in the olfactory
863 bulb and olfactory behaviours. *J Physiol* 602:3519-3543.

864 Christie JM, Bark C, Hormuzdi SG, Helbig I, Monyer H, Westbrook GL (2005)
865 Connexin36 mediates spike synchrony in olfactory bulb glomeruli. *Neuron*
866 46:761-772.

867 Cummings DM, Belluscio L (2010) Continuous neural plasticity in the olfactory
868 intrabulbar circuitry. *J Neurosci* 30:9172-9180.

869 De Saint Jan D, Hirnet D, Westbrook GL, Charpak S (2009) External tufted cells drive
870 the output of olfactory bulb glomeruli. *J Neurosci* 29:2043-2052.

871 Dekker T, Ibba I, Siju KP, Stensmyr MC, Hansson BS (2006) Olfactory shifts parallel
872 superspecialism for toxic fruit in *Drosophila melanogaster* sibling, *D. sechellia*.
873 *Curr Biol* 16:101-109.

874 Dewan A, Cichy A, Zhang J, Miguel K, Feinstein P, Rinberg D, Bozza T (2018) Single
875 olfactory receptors set odor detection thresholds. *Nat Commun* 9:2887.

876 Economo MN, Hansen KR, Wachowiak M (2016) Control of Mitral/Tufted Cell Output by
877 Selective Inhibition among Olfactory Bulb Glomeruli. *Neuron* 91:397-411.

878 Eiting TP, Wachowiak M (2020) Differential Impacts of Repeated Sampling on Odor
879 Representations by Genetically-Defined Mitral and Tufted Cell Subpopulations in
880 the Mouse Olfactory Bulb. *J Neurosci* 40:6177-6188.

881 Ghijzen WE, Leenders AG, Wiegant VM (2001) Regulation of cholecystokinin release
882 from central nerve terminals. *Peptides* 22:1213-1221.

883 Gire DH, Zak JD, Bourne JN, Goodson NB, Schoppa NE (2019) Balancing
884 Extrasynaptic Excitation and Synaptic Inhibition within Olfactory Bulb Glomeruli.
885 *eNeuro* 6.

886 Gire DH, Franks KM, Zak JD, Tanaka KF, Whitesell JD, Mulligan AA, Hen R, Schoppa
887 NE (2012) Mitral cells in the olfactory bulb are mainly excited through a multistep
888 signaling path. *J Neurosci* 32:2964-2975.

889 Griff ER, Mafhouz M, Chaput MA (2008) Comparison of identified mitral and tufted cells
890 in freely breathing rats: II. Odor-evoked responses. *Chem Senses* 33:793-802.

891 Griff IC, Reed RR (1995) The genetic basis for specific anosmia to isoamyl acetate in the
892 mouse. *Cell* 83:407-414.

893 Guitton C, Abbar M, Kinowski JM, Chabrand P, Bressolle F (1998) Multiple-dose
894 pharmacokinetics of clozapine in patients with chronic schizophrenia. *J Clin*
895 *Psychopharmacol* 18:470-476.

896 Hanak AS, Chevillard L, Lebeau R, Risede P, Laplanche JL, Benturquia N, Megarbane
897 B (2017) Neurobehavioral effects of lithium in the rat: Investigation of the
898 effect/concentration relationships and the contribution of the poisoning pattern.
899 *Prog Neuropsychopharmacol Biol Psychiatry* 76:124-133.

900 Hayar A, Karnup S, Shipley MT, Ennis M (2004) Olfactory bulb glomeruli: external tufted
901 cells intrinsically burst at theta frequency and are entrained by patterned olfactory
902 input. *J Neurosci* 24:1190-1199.

903 Hinds JW (1970) Reciprocal and serial dendrodendritic synapses in the glomerular layer
904 of the rat olfactory bulb. *Brain Res* 17:530-534.

905 Hirata T (2024) Olfactory information processing viewed through mitral and tufted cell-
906 specific channels. *Front Neural Circuits* 18:1382626.

907 Igarashi KM, Ieki N, An M, Yamaguchi Y, Nagayama S, Kobayakawa K, Kobayakawa R,
908 Tanifuji M, Sakano H, Chen WR, Mori K (2012) Parallel mitral and tufted cell
909 pathways route distinct odor information to different targets in the olfactory
910 cortex. *J Neurosci* 32:7970-7985.

911 Jendryka M, Palchadhuri M, Ursu D, van der Veen B, Liss B, Katzel D, Nissen W,
912 Pekcec A (2019) Pharmacokinetic and pharmacodynamic actions of clozapine-N-
913 oxide, clozapine, and compound 21 in DREADD-based chemogenetics in mice.
914 *Sci Rep* 9:4522.

915 Jones S, Zylberberg J, Schoppa N (2020) Cellular and Synaptic Mechanisms That
916 Differentiate Mitral Cells and Superficial Tufted Cells Into Parallel Output
917 Channels in the Olfactory Bulb. *Front Cell Neurosci* 14:614377.

918 Kosaka T, Kosaka K (2004) Neuronal gap junctions between intraglomerular
919 mitral/tufted cell dendrites in the mouse main olfactory bulb. *Neurosci Res*
920 49:373-378.

921 Kosaka T, Kosaka K (2005) Intraglomerular dendritic link connected by gap junctions
922 and chemical synapses in the mouse main olfactory bulb: electron microscopic
923 serial section analyses. *Neuroscience* 131:611-625.

924 Liu S, Shipley MT (2008) Multiple conductances cooperatively regulate spontaneous
925 bursting in mouse olfactory bulb external tufted cells. *J Neurosci* 28:1625-1639.

926 Liu S, Puche AC, Shipley MT (2016) The Interglomerular Circuit Potently Inhibits
927 Olfactory Bulb Output Neurons by Both Direct and Indirect Pathways. *J Neurosci*
928 36:9604-9617.

929 Liu S, Plachez C, Shao Z, Puche A, Shipley MT (2013) Olfactory bulb short axon cell
930 release of GABA and dopamine produces a temporally biphasic inhibition-
931 excitation response in external tufted cells. *J Neurosci* 33:2916-2926.

932 Liu WL, Shipley MT (1994) Intrabulbar associational system in the rat olfactory bulb
933 comprises cholecystinin-containing tufted cells that synapse onto the dendrites
934 of GABAergic granule cells. *J Comp Neurol* 346:541-558.

935 Liu X, Liu S (2018) Cholecystinin selectively activates short axon cells to enhance
936 inhibition of olfactory bulb output neurons. *J Physiol* 596:2185-2207.

937 Lledo PM, Gheusi G, Vincent JD (2005) Information processing in the mammalian
938 olfactory system. *Physiol Rev* 85:281-317.

939 Lodovichi C, Belluscio L, Katz LC (2003) Functional topography of connections linking
940 mirror-symmetric maps in the mouse olfactory bulb. *Neuron* 38:265-276.

941 Machado CF, Reis-Silva TM, Lyra CS, Felicio LF, Malnic B (2018) Buried Food-seeking
942 Test for the Assessment of Olfactory Detection in Mice. *Bio Protoc* 8:e2897.

943 Macrides F, Schneider SP (1982) Laminar organization of mitral and tufted cells in the
944 main olfactory bulb of the adult hamster. *J Comp Neurol* 208:419-430.

945 Markopoulos F, Rokni D, Gire DH, Murthy VN (2012) Functional properties of cortical
946 feedback projections to the olfactory bulb. *Neuron* 76:1175-1188.

947 Marks CA, Cheng K, Cummings DM, Belluscio L (2006) Activity-dependent plasticity in
948 the olfactory intrabulbar map. *J Neurosci* 26:11257-11266.

949 Meisami E (1989) A proposed relationship between increases in the number of olfactory
950 receptor neurons, convergence ratio and sensitivity in the developing rat. *Brain*
951 *Res Dev Brain Res* 46:9-19.

952 Mombaerts P, Wang F, Dulac C, Chao SK, Nemes A, Mendelsohn M, Edmondson J,
953 Axel R (1996) Visualizing an olfactory sensory map. *Cell* 87:675-686.

954 Mori K, Sakano H (2021) Olfactory Circuitry and Behavioral Decisions. *Annu Rev*
955 *Physiol* 83:231-256.

956 Nagayama S, Homma R, Imamura F (2014) Neuronal organization of olfactory bulb
957 circuits. *Front Neural Circuits* 8:98.

958 Najac M, De Saint Jan D, Reguero L, Grandes P, Charpak S (2011) Monosynaptic and
959 polysynaptic feed-forward inputs to mitral cells from olfactory sensory neurons. *J*
960 *Neurosci* 31:8722-8729.

961 Orona E, Rainer EC, Scott JW (1984) Dendritic and axonal organization of mitral and
962 tufted cells in the rat olfactory bulb. *J Comp Neurol* 226:346-356.

963 Ossenkopp KP, Eckel LA (1995) Toxin-induced conditioned changes in taste reactivity
964 and the role of the chemosensitive area postrema. *Neurosci Biobehav Rev*
965 19:99-108.

966 Pourtier L, Sicard G (1990) Comparison of the sensitivity of C57BL/6J and AKR/J mice
967 to airborne molecules of isovaleric acid and amyl acetate. *Behav Genet* 20:499-
968 509.

969 Ressler KJ, Sullivan SL, Buck LB (1994) Information coding in the olfactory system:
970 evidence for a stereotyped and highly organized epitope map in the olfactory
971 bulb. *Cell* 79:1245-1255.

972 Rubin BD, Katz LC (1999) Optical imaging of odorant representations in the mammalian
973 olfactory bulb. *Neuron* 23:499-511.

974 Schoenfeld TA, Marchand JE, Macrides F (1985) Topographic organization of tufted cell
975 axonal projections in the hamster main olfactory bulb: an intrabulbar
976 associational system. *J Comp Neurol* 235:503-518.

977 Seibenhener ML, Wooten MC (2015) Use of the Open Field Maze to measure
978 locomotor and anxiety-like behavior in mice. *J Vis Exp*:e52434.

979 Serogy KB, Brecha N, Gall C (1985) Distribution of cholecystinin-like
980 immunoreactivity in the rat main olfactory bulb. *J Comp Neurol* 239:373-383.

981 Shao Z, Puche AC, Liu S, Shipley MT (2012) Intraglomerular inhibition shapes the
982 strength and temporal structure of glomerular output. *J Neurophysiol* 108:782-
983 793.

984 Shao Z, Puche AC, Kiyokage E, Szabo G, Shipley MT (2009) Two GABAergic
985 intraglomerular circuits differentially regulate tonic and phasic presynaptic
986 inhibition of olfactory nerve terminals. *J Neurophysiol* 101:1988-2001.

987 Short SM, Wachowiak M (2019) Temporal Dynamics of Inhalation-Linked Activity across
988 Defined Subpopulations of Mouse Olfactory Bulb Neurons Imaged In Vivo.
989 *eNeuro* 6.

990 Sun X, Liu X, Starr ER, Liu S (2020) CCKergic Tufted Cells Differentially Drive Two
991 Anatomically Segregated Inhibitory Circuits in the Mouse Olfactory Bulb. *J*
992 *Neurosci* 40:6189-6206.

993 van Drongelen W, Holley A, Doving KB (1978) Convergence in the olfactory system:
994 quantitative aspects of odour sensitivity. *J Theor Biol* 71:39-48.

995 Vassar R, Chao SK, Sitcheran R, Nunez JM, Vosshall LB, Axel R (1994) Topographic
996 organization of sensory projections to the olfactory bulb. *Cell* 79:981-991.
997 Wysocki CJ, Whitney G, Tucker D (1977) Specific anosmia in the laboratory mouse.
998 *Behav Genet* 7:171-188.
999 Yang M, Crawley JN (2009) Simple behavioral assessment of mouse olfaction. *Curr*
1000 *Protoc Neurosci* Chapter 8:Unit 8 24.
1001 Zak JD, Schoppa NE (2021) Optical Manipulations Reveal Strong Reciprocal Inhibition
1002 But Limited Recurrent Excitation within Olfactory Bulb Glomeruli. *eNeuro* 8.
1003 Zhou Z, Belluscio L (2008) Intrabulbar projecting external tufted cells mediate a timing-
1004 based mechanism that dynamically gates olfactory bulb output. *J Neurosci*
1005 28:9920-9928.
1006 Zou DJ, Chesler A, Firestein S (2009) How the olfactory bulb got its glomeruli: a just so
1007 story? *Nat Rev Neurosci* 10:611-618.

1008

1009

1010

1011

1012

1013

1014

1015

1016

1017

1018

1019

Figure Legends

1020

1021 **Fig 1.** Preferential labeling of OB superficial tufted cells. **A**, confocal imaging of a
1022 coronal OB section from a CCK-Cre mouse 4 weeks after AAV5-FLEX-tdTomato
1023 injection into the medial side of the bulb. Predominant tdTomato fluorescence is notable
1024 in the superficial EPL on the medial side and IPL of the whole bulb. **B**, a zoom-in photo
1025 from A showing only a few of cells are labeled in the glomerular layer. **C & D**, zoom-in
1026 photos from A highlighting examples of deep (dTTC, C) and middle tufted cells (mTC, D)
1027 labeled. **E**, zoom-in photo from C showing representative labeling of superficial (sTCs)
1028 and external tufted cells (eTCs) in the EPL or the glomerular layer. **F**, quantified data
1029 showing the percentage of each subpopulation of tufted cells are labeled with our
1030 approach.

1031 **Fig 2.** AMPA and NMDA receptors mediate the ON-evoked CCKergic STC response. **A**,
1032 left: confocal image of a coronal OB section showing the expression of ChR2-EYFP
1033 (green) predominantly in the CCKergic STCs with somata located in the superficial EPL,
1034 apical dendrites ramifying in individual glomeruli, and axons traveling and confined to
1035 the IPL. The section was counterstained with DAPI (white). Right: blown-up photo from
1036 A to highlight ChR2-EYFP expression in the different layers. D: dorsal, V: ventral, M:
1037 medial, L: lateral, EPL: external plexiform layer, GCL: granule cell layer, GL: glomerular
1038 layer; IPL: internal plexiform layer, MCL: mitral cell layer, ONL: olfactory nerve layer. **B**,
1039 top: schematic of experimental design; bottom: confocal image of a typical sTC (red)
1040 recorded and filled with biocytin reconstructed by immunohistochemical staining. Note a
1041 single primary/apical dendrite ramifying in one glomerulus and a secondary dendrite
1042 running laterally. **C & D**, Typical voltage (C) or current clamp (D) traces recorded from

1043 an EYFP-labeled CCKergic STC showing the ON-evoked responses in ACSF (black), in
1044 the presence of APV (red) or DNQX and APV (green). **E-H**, Bar graphs representing
1045 quantified data of the ON-evoked responses in the CCKergic STCs in terms of charge
1046 or amplitude (F) of EPSCs, burst duration (G) or number of action potentials (AP, H) in
1047 ACSF, or in the presence of APV or APV+DNQX. * $p < 0.05$; ** $p < 0.01$; *** $p < 0.001$.

1048 **Fig 3.** CCKergic STCs provide long-lasting excitation to MCs via dendrodendritic
1049 transmission in the glomerulus. **A**, left: illustration of experimental design; right: photo of
1050 a recorded mitral cell filled by the fluorescent dye Alexa 594 via the patch clamp
1051 recording pipette. EPL: external plexiform layer, GL: glomerular layer; IPL: internal
1052 plexiform layer, MCL: mitral cell layer, ONL: olfactory nerve layer. **B**, Representative
1053 voltage clamp recording traces showing the long-lasting MC response to optogenetic
1054 activation of CCKergic STC apical dendrites in the glomerulus in ACSF (black) or after
1055 bath application of APV (red) or APV and DNQX (Green). Blue arrow denoting blue light
1056 stimulation. **C-E**, Pooled data of 7 cells showing the onset latencies (C), charge (D) or
1057 initial peak amplitude (E) of the STC-evoked MC responses under different conditions
1058 as shown in B. **F**, Representative current clamp recording traces showing the long-
1059 lasting MC response to optogenetic activation of CCKergic STC apical dendrites in the
1060 glomerulus in ACSF (black) or after bath application of APV (red) or APV and DNQX
1061 (Green). **G & H**, Pooled data of 5 cells showing the number of action potentials (G) or
1062 spike burst duration (H) of the STC-evoked MC responses under different conditions as
1063 shown in F. * $p < 0.05$; ** $p < 0.01$; *** $p < 0.001$.

1064 **Fig 4.** Expression and function of halorhodopsin (NpHR) in CCKergic STCs. **A**, Left:
1065 confocal image of a horizontal OB section showing NpHR-EYFP expression

1066 predominantly in STCs; Right: blow-up of the area within the red square from the left.
1067 EPL: external plexiform layer, GCL: granule cell layer, GL: glomerular layer; IPL:
1068 internal plexiform layer, MCL: mitral cell layer, ONL: olfactory nerve layer. **B**,
1069 representative recording traces from an EYFP-expressing STC in voltage (top) or
1070 current (bottom) clamp showing the outward currents or hyperpolarization elicited by a
1071 200 ms or 2 s green light (590 nm) exposure to the recorded cell body.

1072 **Fig 5.** Optic inhibition of the CCKergic STC apical dendrites significantly attenuates the
1073 ON-evoked MC response. **A**, left: schematic of experimental design; right: photo of a
1074 recorded mitral cell filled by the fluorescent dye Alexa 594 via the patch clamp recording
1075 pipette. EPL: external plexiform layer, GCL: granule cell layer, GL: glomerular layer;
1076 IPL: internal plexiform layer, MCL: mitral cell layer, ONL: olfactory nerve layer. **B**,
1077 Representative current clamp traces showing MC responses to ON stimulation (black
1078 arrow head) before (top trace) or after (middle trace) green light stimulation was turned
1079 on to activate the NpHR in STCs. Bottom trace is a blow-up of the middle trace to
1080 highlight the hyperpolarization during green light exposure. Arrow head: olfactory nerve
1081 stimulation (ON stim). **C & D**, Data pooled from 9 MCs showing the effects of light
1082 stimulation on the burst duration and number of action potentials (APs) of MC
1083 responses to ON stimulation. *** $p < 0.001$.

1084 **Fig 6.** Gap junction contributes to the ON-evoked excitatory response in MCs. **A&C**,
1085 left: schematic illustration of the design of experiments shown in B & D, respectively; right:
1086 photos of recorded mitral cells filled by the fluorescent dye Alexa 594 via the patch
1087 clamp recording pipette. EPL: external plexiform layer, GCL: granule cell layer, GL:
1088 glomerular layer; IPL: internal plexiform layer, MCL: mitral cell layer, ONL: olfactory

1089 nerve layer. **B**, Typical voltage clamp traces showing responses of a MC in the
1090 presence of 10 μ M NBQX and 50 μ M APV (black) or after (purple) addition of the gap
1091 junction blocker carbenoxolone (CBX, 300 μ M). **D**, Top: Typical voltage traces showing
1092 MC responses to the green light stimulation presented to activate NpHR and inhibit STC
1093 apical dendrites in the glomerulus receiving the apical dendrite of the recorded MC as
1094 shown in C in the presence of NBQX & APV (black) or with addition of CBX (purple).
1095 Bottom: a blow-up of the response portion highlighted with gray color shown in the top
1096 panel. **E**, Bar graphs representing quantified data comparing the ON stimulation-evoked
1097 (E) or light stimulation-evoked (F) MC responses charge in the presence of NBQX &
1098 APV (black) or with addition of CBX (purple), respectively. **F**, time course effects of CBX
1099 (n=6 cells) on the integrated charge of both inward and outward current by comparing to
1100 control cells (n=5). * $p < 0.05$, *** $p < 0.01$, **** $p < 0.001$.

1101 **Fig 7.** Optogenetic inhibition of CCKergic STCs drastically reduces the ON-evoked MC
1102 responses in the presence of CBX. **A**, left: experimental setup; right: photo of a
1103 recorded mitral cell filled by the fluorescent dye Alexa 594 via the patch clamp recording
1104 pipette. **B**, Representative current clamp recording traces showing MC responses to ON
1105 electrical stimulation in the absence (gray) or presence (green) of green light stimulation
1106 presented to the glomerulus affiliated by the apical dendrite of the recorded MC to
1107 activate NpHR and inhibit the CCKergic STC apical dendrites as shown in A. **C&D**,
1108 Population data showing the number of action potentials (APs) (C) and burst duration
1109 (D) of the ON-evoked MC responses in the absence (control) or presence of light
1110 stimulation (HR). ** $p < 0.01$.

1111 **Fig 8.** CCKergic STCs activate MCs on the opposite side of same OB via axons in the
1112 IPL. **A**, Illustration of experimental design on a confocal image of a coronal section of
1113 OB where ChR2-mCherry (red) was expressed in CCKergic STCs on the medial side.
1114 Note: mCherry expression only in the IPL on the lateral side, indicating axon projection
1115 from the CCKergic STCs on the medial side. **B**, Epifluorescence microscopic photo
1116 showing a recorded MC with a truncated apical dendrite and filled by Alexa Fluor 594
1117 via the patch pipette. **C**, Typical voltage clamp traces showing responses a MC on the
1118 lateral side to the optical stimulation presented to the IPL right beneath as shown in A in
1119 ACSF (black), APV (red) or APV&NBQX (green). **D&E**, Bar graphs of quantified data
1120 showing the charge (D) and amplitude (E) of EPSCs in 8 MCs on the lateral side of the
1121 OB evoked by optical stimulation presented to the underneath IPL in ACSF (black), APV
1122 (red), or APV+DNQX (green). **F**, Onset latencies of the EPSCs in 8 MCs. * $p < 0.05$; **
1123 $p < 0.01$.

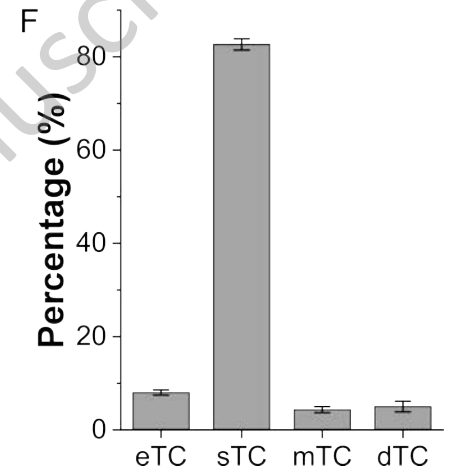
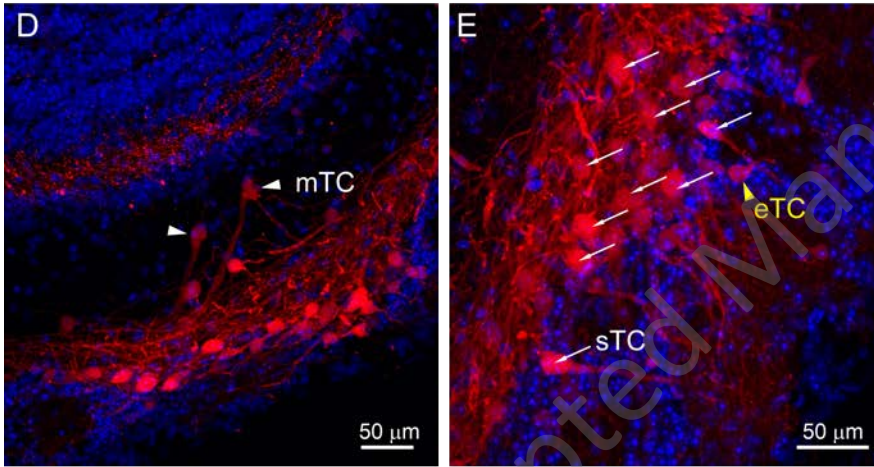
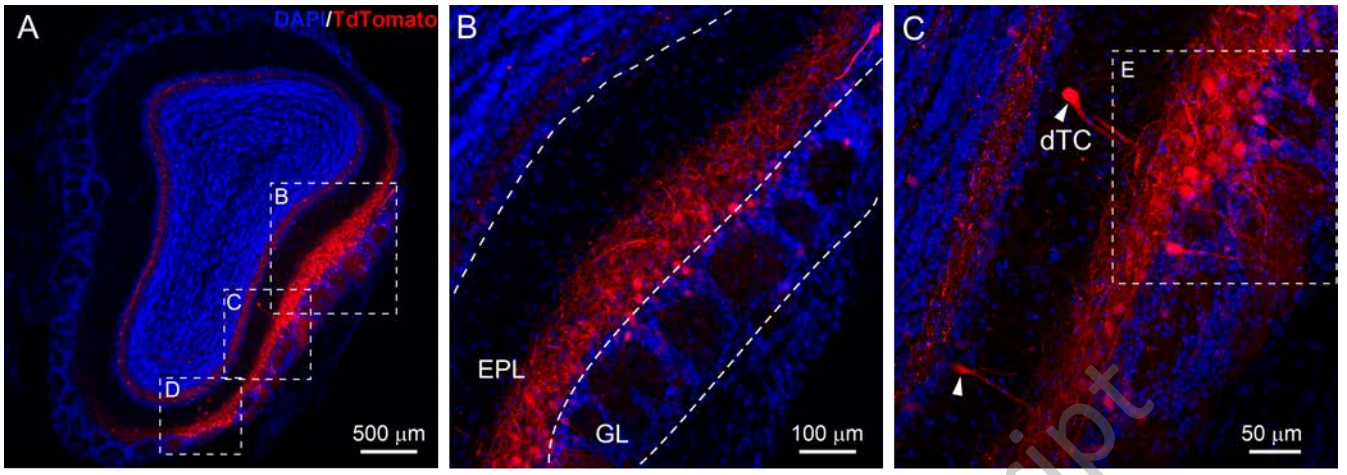
1124 **Fig 9.** Expression and function of the inhibitory DREADD (hM4Di)-mCherry in the
1125 CCKergic STCs. **A**, left: confocal image of a coronal OB section showing DREAD-
1126 mCherry (red) expression predominantly in the glomerular layer, superficial EPL, and
1127 IPL, counterstained with DAPI (white). Right: blown-up from A. EPL: external plexiform
1128 layer, GCL: granule cell layer, GL: glomerular layer; IPL: internal plexiform layer, MCL:
1129 mitral cell layer. **B**, Typical current clamp traces showing responses of a mCherry-
1130 expressing STC to the bath-applied DREADD actuator clozapine-N-oxide (CNO, 10
1131 μ M). Note: spontaneous action potentials were terminated and membrane was
1132 hyperpolarized by CNO as shown by the insert. **C&D**, Pooled data from 5 cells showing

1133 the effects of CNO on spontaneous firing rate (C) and minimal membrane potential
1134 (MMP, D). * $p < 0.05$; *** $p < 0.001$.

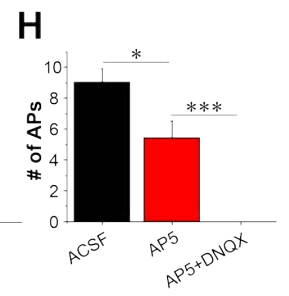
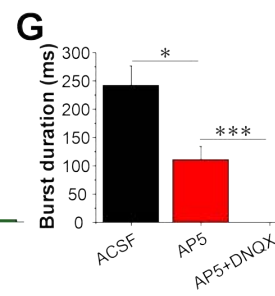
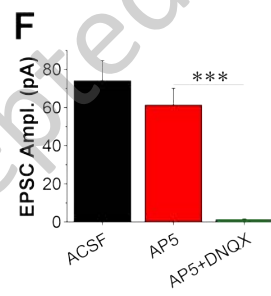
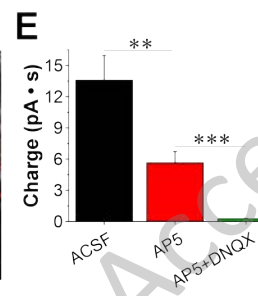
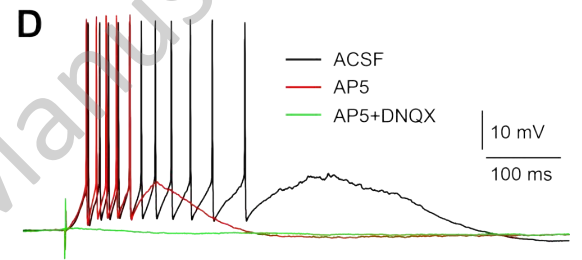
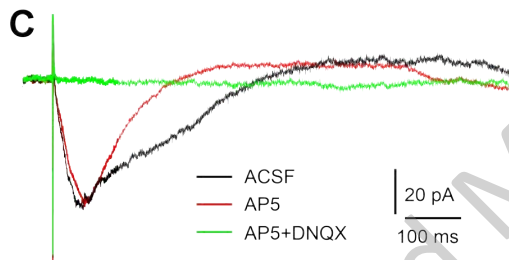
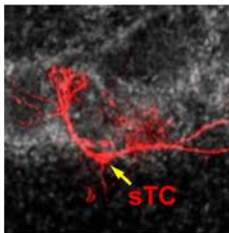
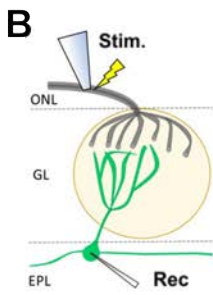
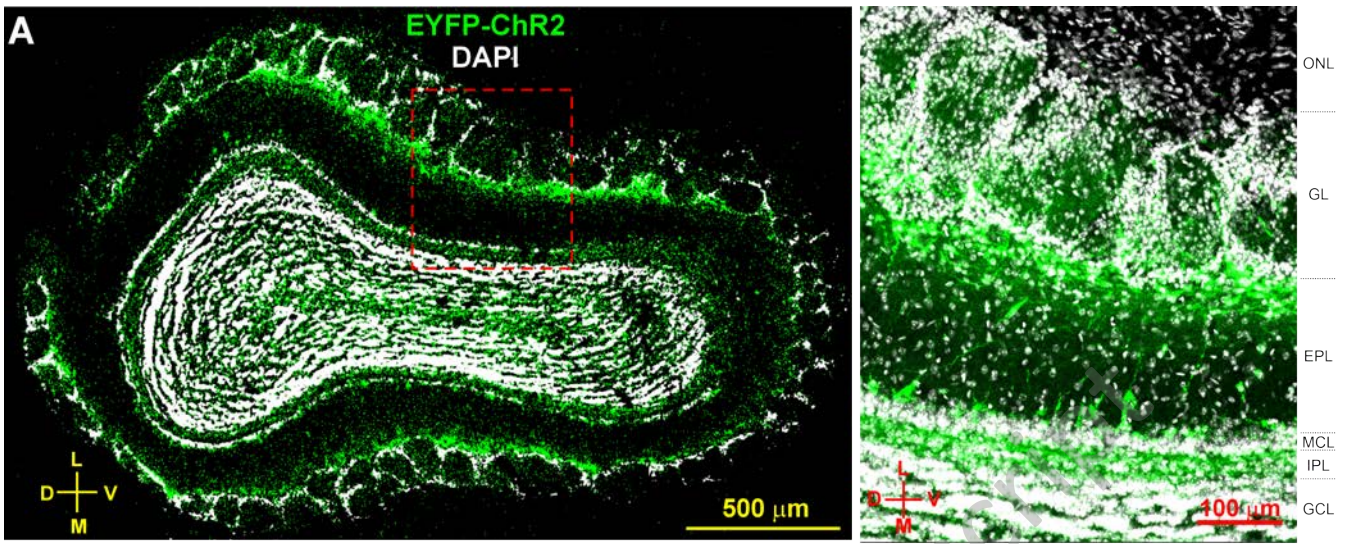
1135 **Fig 10.** Chemogenetic inhibition of the CCKergic STCs reduces animal's sensitivity to
1136 food odors. **A**, Time course illustration of the experimental design. **B&C**, Bar graphs
1137 showing the latencies for identifying the buried (B) or visible (C) food in the behavioral
1138 test in four groups of mice. **D&E**, Bar graphs comparing the traveling distance in the
1139 whole testing arena (D) or the central zone (E) in the open field test behavioral test
1140 among four groups of mice. *** $p < 0.001$.

1141 **Fig 11.** Chemogenetic inhibition of the CCKergic STCs elevates animal's detection
1142 threshold for isovaleric acid (iVA). **A**, Time course illustration of the experimental
1143 design. **B**, Symbol-line graph comparing the iVA preference index among four groups of
1144 mice exposed to 5 decreasing concentrations (10^{-3} M to 10^{-7} M) of iVA in 5 consecutive
1145 testing days. N=13 mice/group, # $p < 0.05$ compared to DREAD/saline or ChR2/CNO
1146 group, ** $p < 0.01$ & *** $p < 0.001$ compared to any of the other groups.

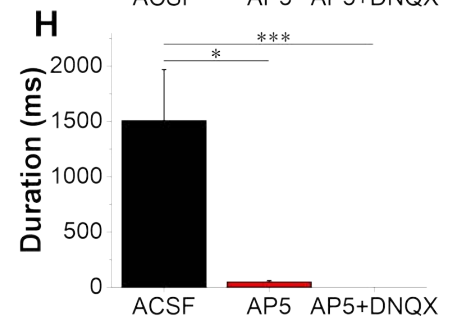
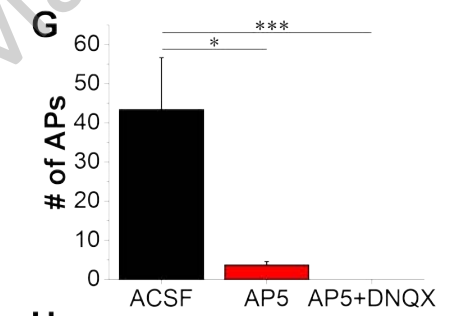
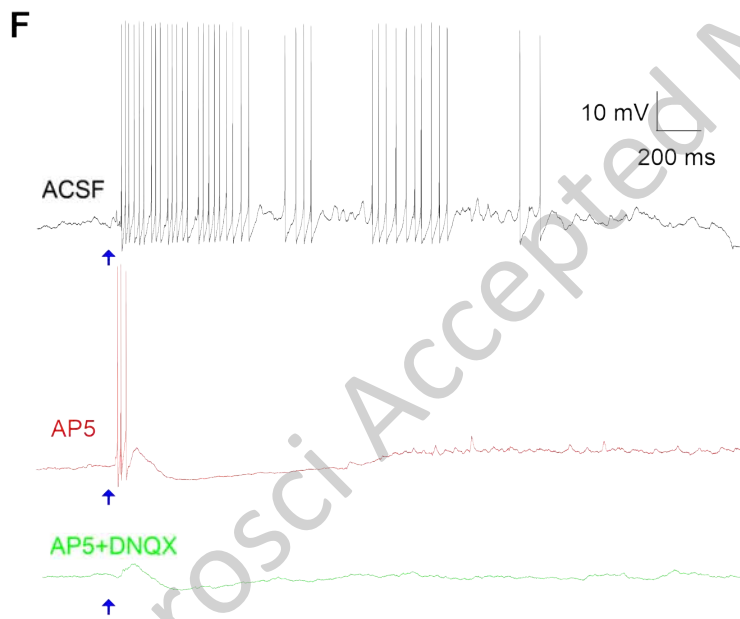
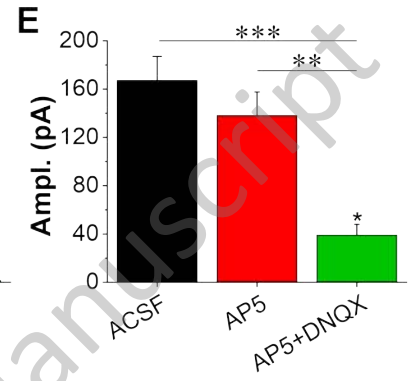
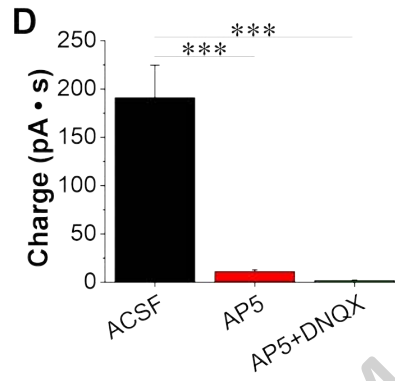
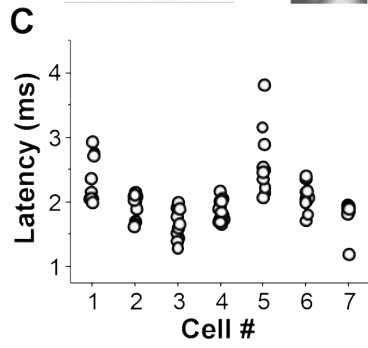
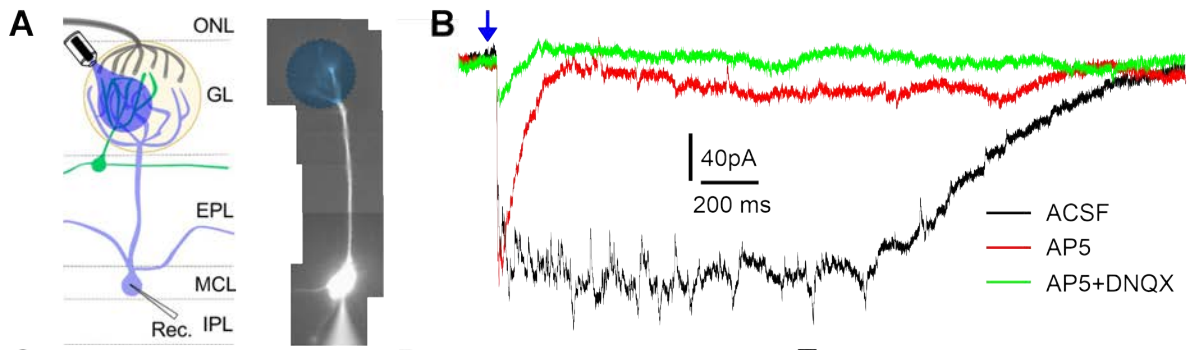
1147 **Fig 12.** Speculative summary of CCKergic TC actions on MC output. **A**, STCs receive
1148 direct excitatory input from OSNs (1) and intermediate the excitatory input to MCs via
1149 apical dendrites (2) and provide excitatory feedforward to MCs on the opposite side the
1150 same OB via their axon terminals in the IPL (3). **B**, Illustration of summation of the
1151 subthreshold orthodromic synaptic response (EPSP) evoked apical dendrites of STCs
1152 on the same side and subthreshold antidromic synaptic response (EPSP) elicited by
1153 axons of STCs on the opposite side to trigger a suprathreshold output response (action
1154 potential, AP) in the MC.



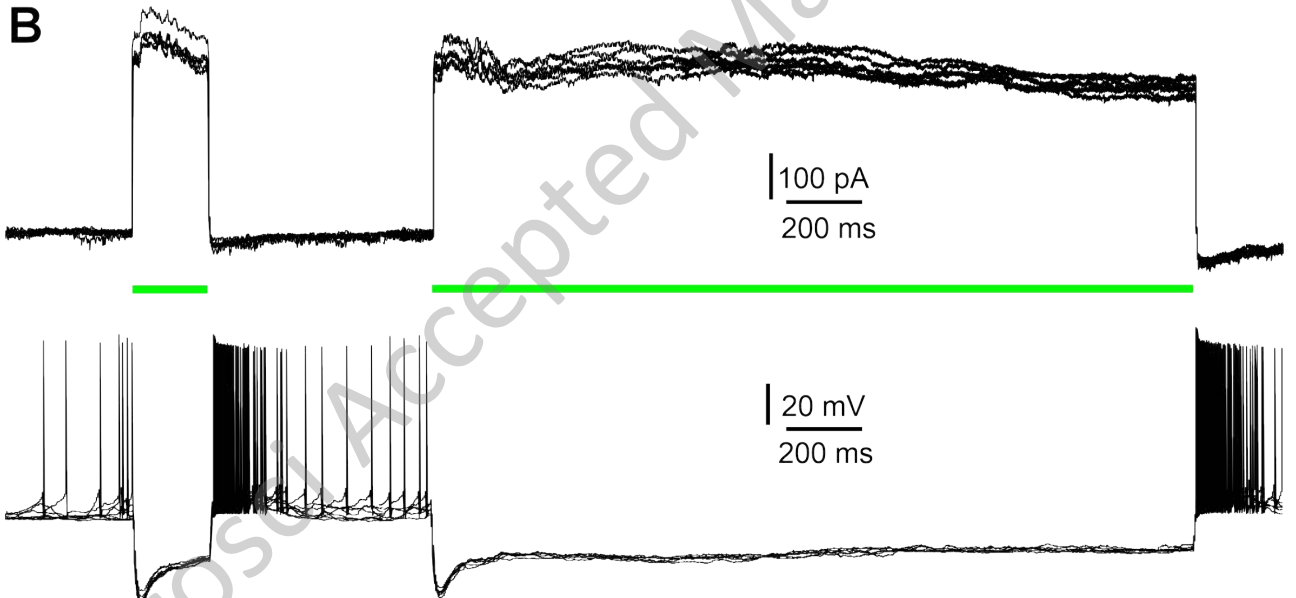
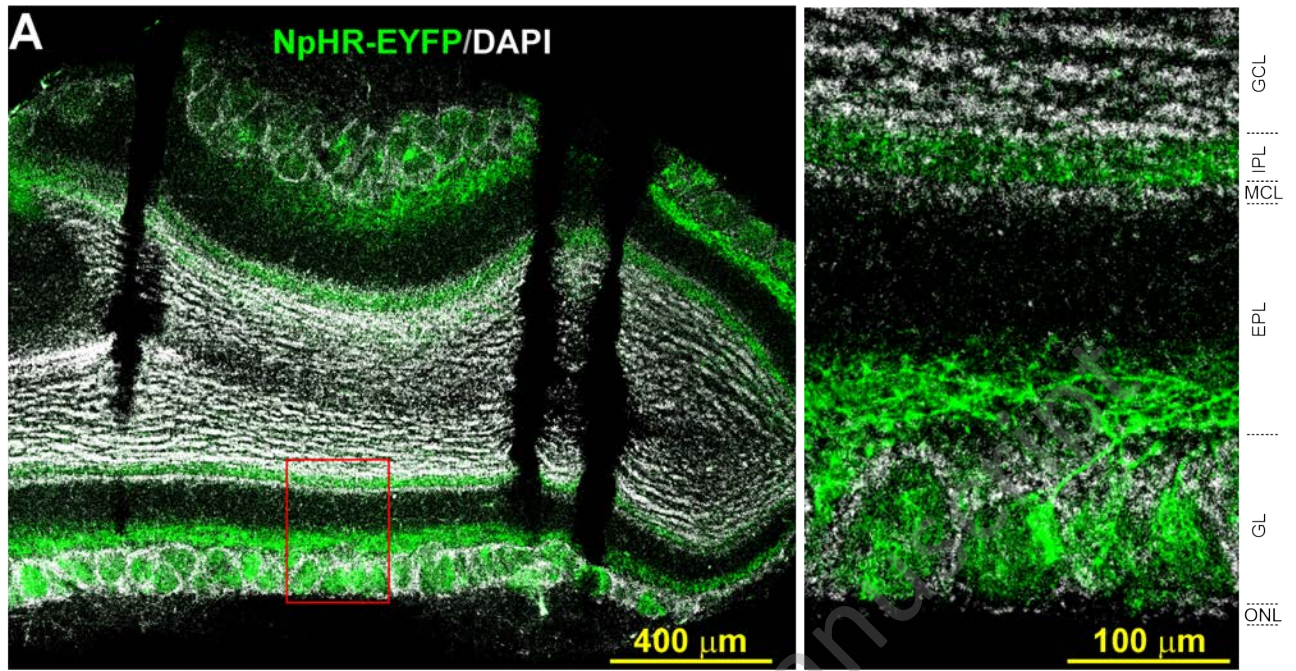
JNeurosci Accepted Manuscript

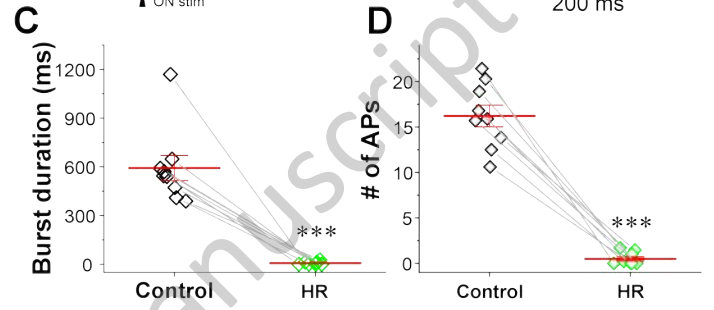
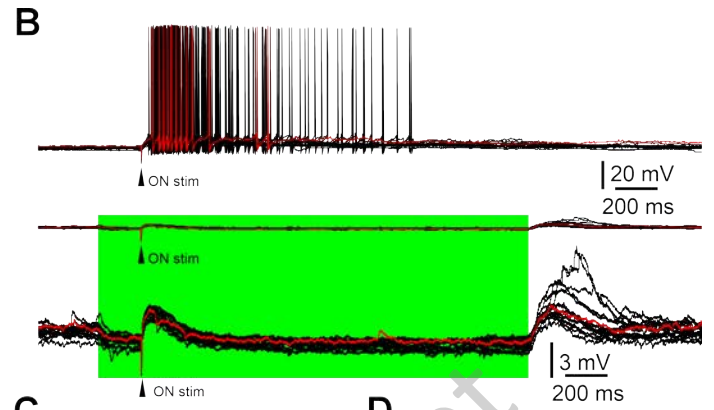
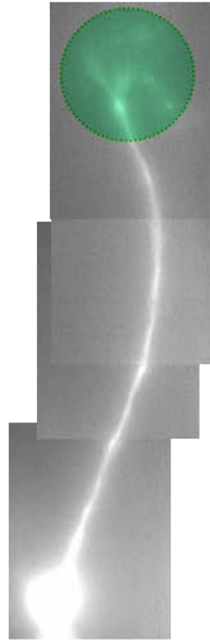
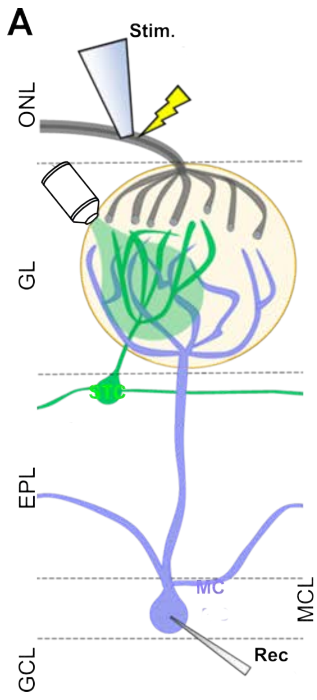


JNeurosci Accepted Manuscript

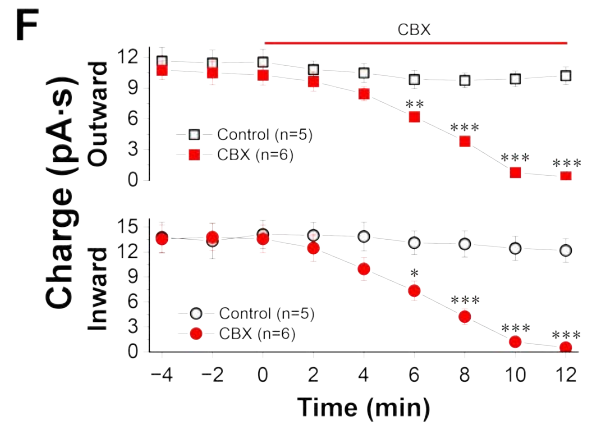
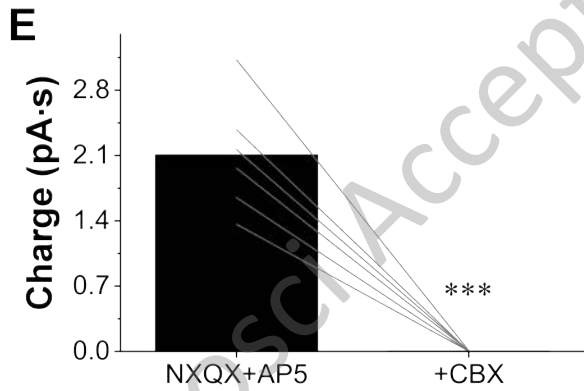
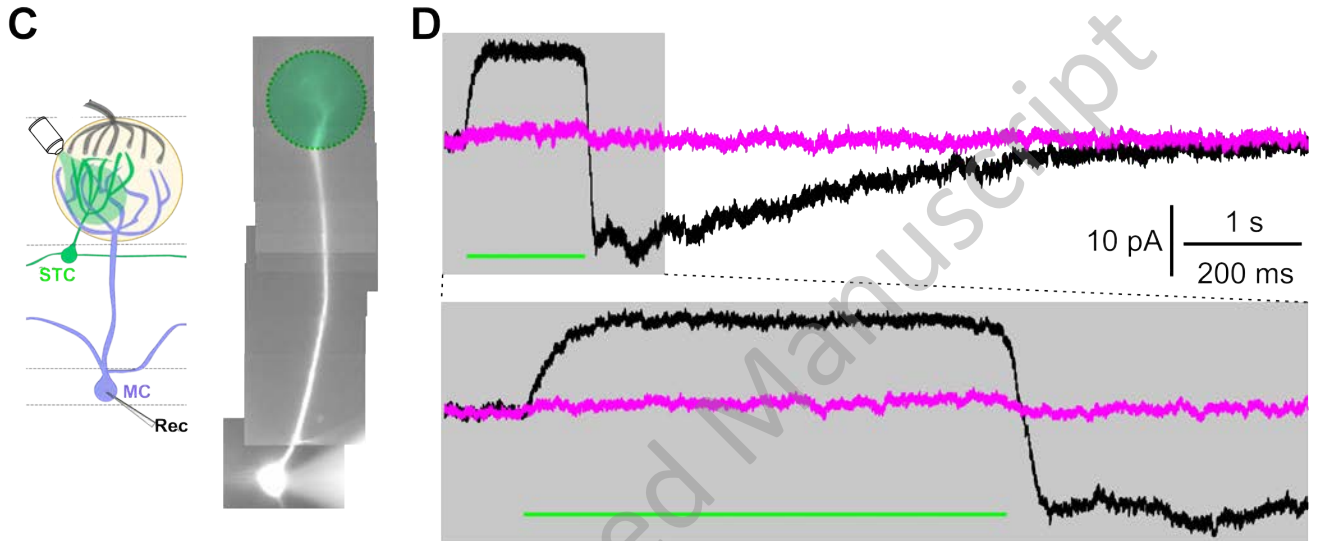
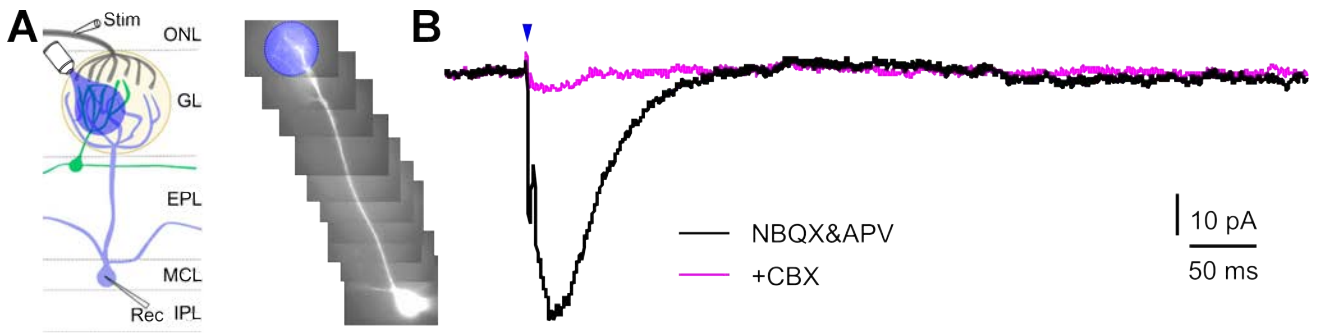


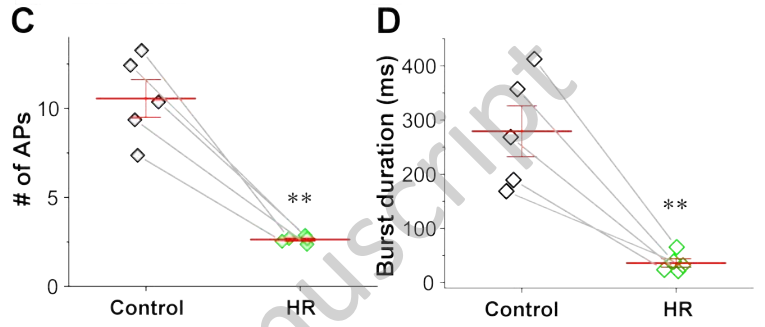
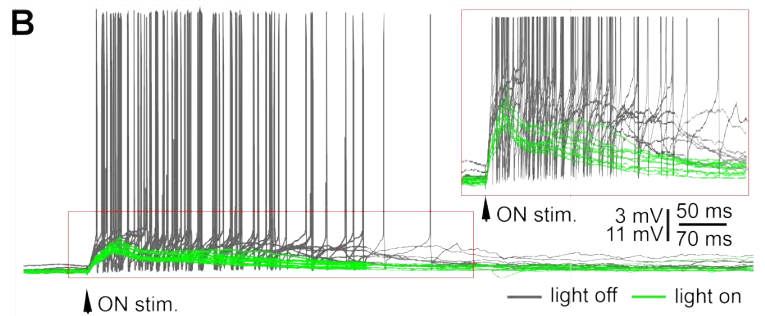
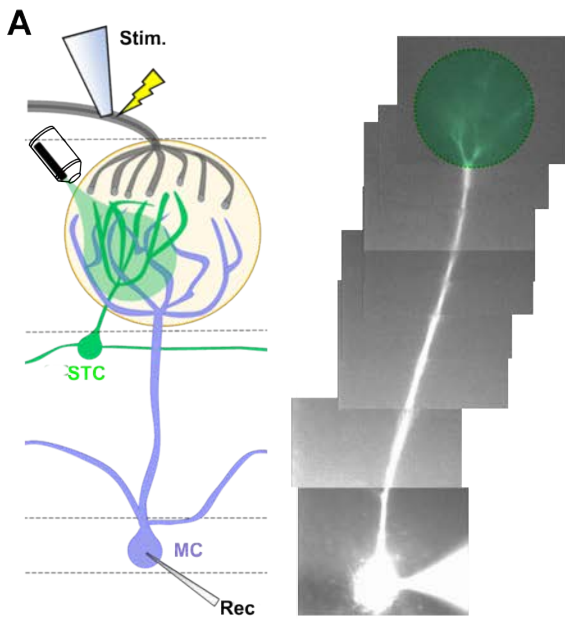
Accepted Manuscript



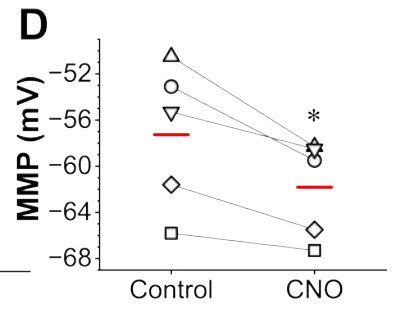
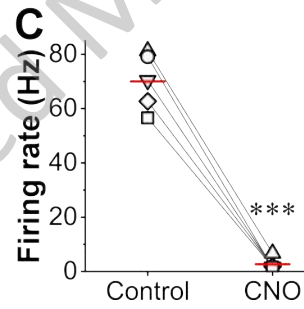
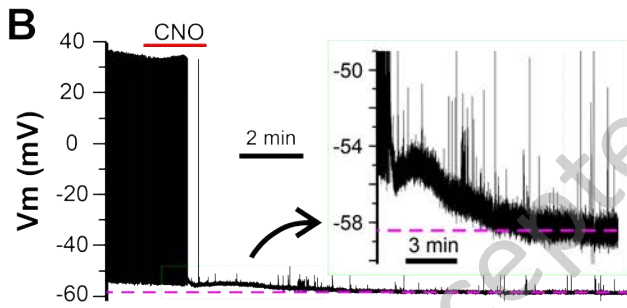
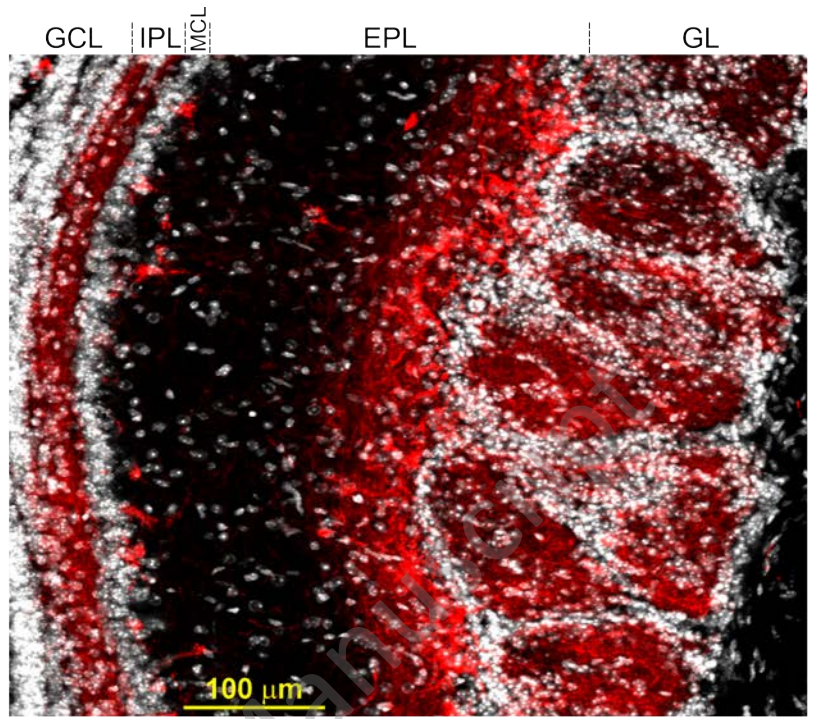
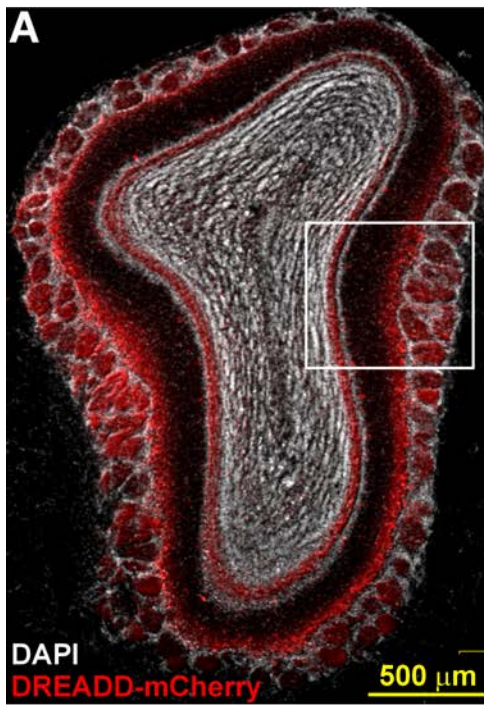


JNeurosci Accepted Manuscript

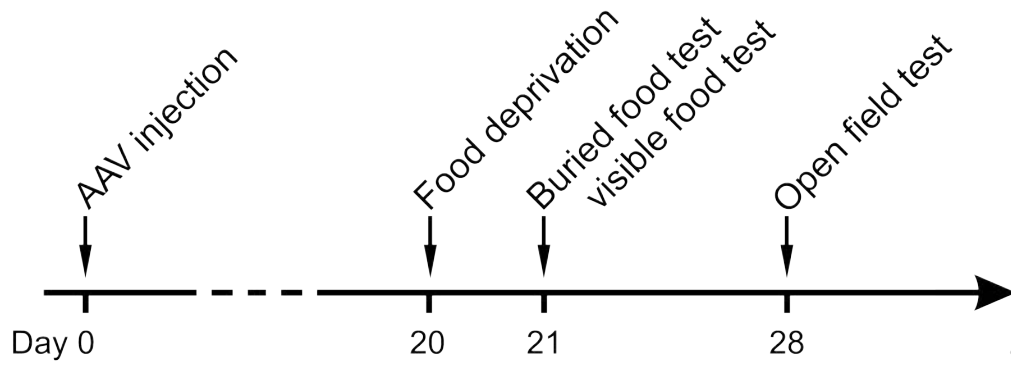
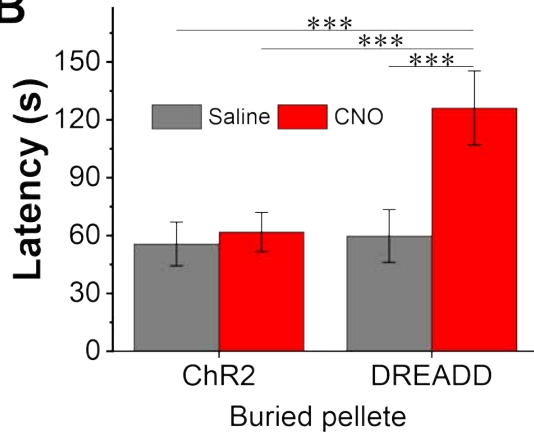
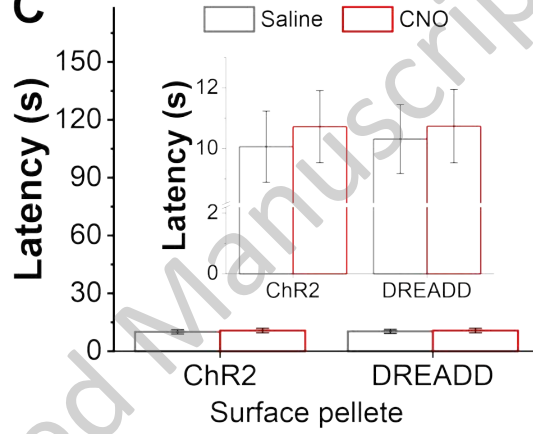
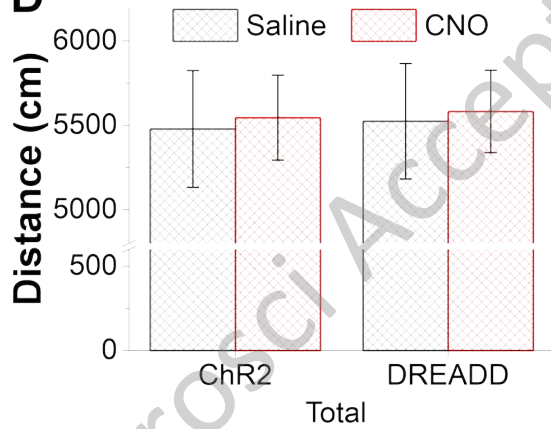
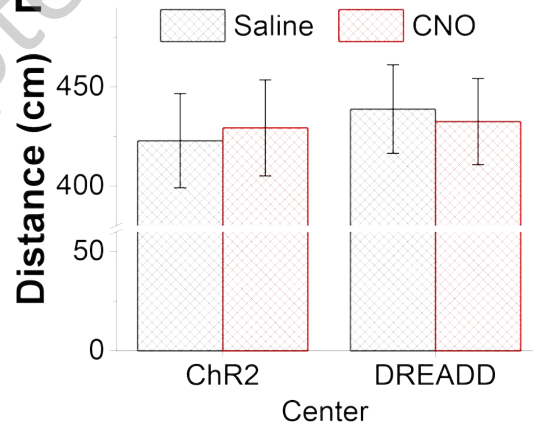


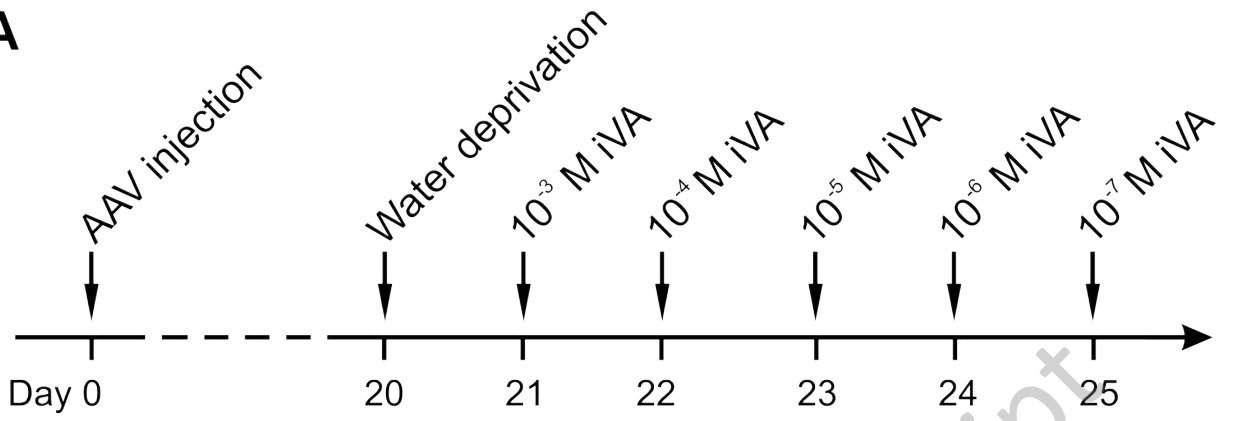
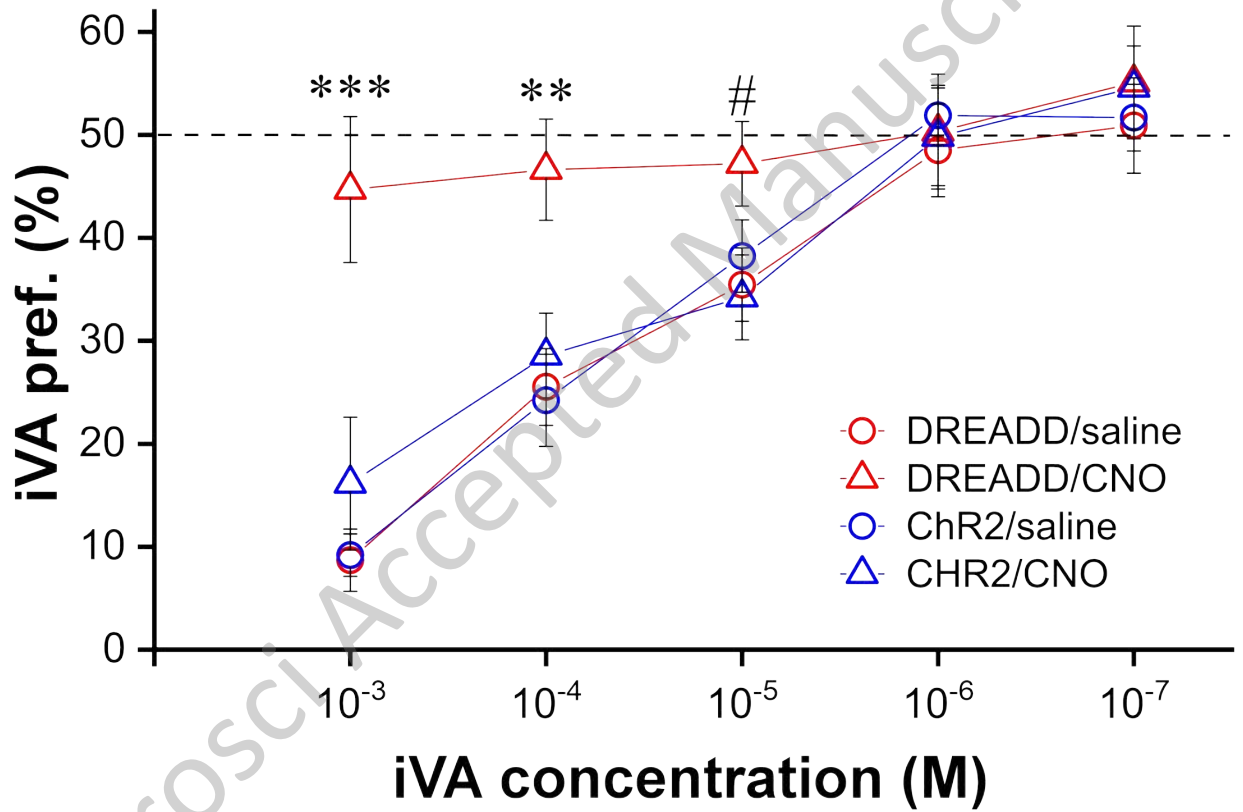


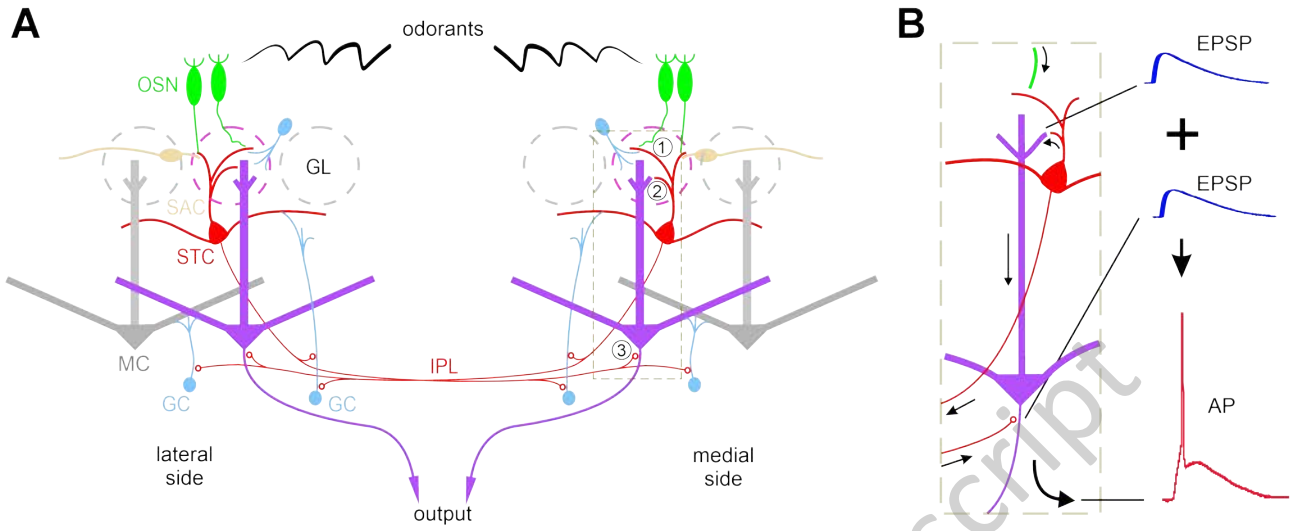
JNeurosci Accepted Manuscript



JNeurosci Accepted Manuscript

A**B****C****D****E**

A**B**



JNeurosci Accepted Manuscript